Journal of Neurology & Neurophysiology
ISSN: 2155-9562

von Wild et al., J Neurol Neurophysiol 2017, 8:5
DOI: 10.4172/2155-9562.1000450

Research Article Open Access

New Aspects of Graft-induced Central Plasticity and Neuroregeneration at T 10 in a Rat Model†

von Wild KRH[1]*, Catoi C[2], Tobias von Wild[3], Giorgio Brunelli[4], Dafin Muresanu[5], Peter Trillenberg[6], Marc Heidbreder[7], Laura Farcas[8], Adrian F Gal[8], Marian A Taulescu[8], Alexandru I Gudea[9], Johannes C Vester[10] and Marlene Löhnhardt[11]*

[1]*Westphalia Wilhelm's University Münster, Münster, Germany*
[2]*Department of Pathology, Rector of University of Agricultural Science and Veterinary Medicine, Cluj Napoca, Romania*
[3]*Department of Plastic Reconstructive and Aesthetic Surgery, Hand Surgery; Praxisklinik in der Alster City, Hamburg, Germany*
[4]*Foundation Giorgio Brunelli for Research on Spinal Cord Lesions, Cellatica, Italy*
[5]*Department of Neurosciences, University of Medicine and Pharmacy Iuliu Hatieganu, Cluj Napoca, Romania*
[6]*Department for Neurology, UK-SH, Campus Luebeck, Germany*
[7]*Department of Pharmacology and Toxicology, Krankenversicherung Nord, Hamburg, Germany*
[8]*Department of Veterinary Pathology, University of Agricultural Sciences and Veterinary Medicine, Cluj-Napoca, Romania*
[9]*Department of Comparative Anatomy, University of Agricultural Sciences and Veterinary Medicine, Cluj Napoca, Romania*
[10]*Department of Biometry and Clinical Research, idv Data Analysis and Study Planning; Konrad-Zuse-Bogen, Germany*
[11]*Clinic and Polyclinic for Accident, Hand and Restorative Surgery, University Hospital Hamburg-Eppendorf Martinistraße, Germany*

†***In Memoriam Geoffrey Raisman, born at June 28. 1939, deceased at January 27. 2017***

Abstract

Objective: Retest Brunelli's graft induced glutamate neurotransmitter switch at the neuromuscular junction in rat for the translation of new aspects of central plasticity concepts for human reconstructive surgery in spinal cord lesions.

Methods: Randomized double blind controlled study in rat, which was limited to 30 animals (Charles River, 220 to 280 g). Ethical research approval was obtained from the Animal Research Committee of the University Hospital Schleswig Holstein, UK-SH, Lübeck, D, and legitimated by the Governmental Department of Agriculture, Natural Environments and Agriculture Kiel, D, in compliance with the European Commission Recommendation to retest and review of graft-induced glutamatergic regeneration and /or cholinergic co-transmission at the neuromuscular junction for reinnervation of the skeletal internal obliquus abdominal muscle fibres. Assessments were performed to demonstrate pharmacological neuromodulation after attaching the lateral corticospinal tract at T10 to the bisected skeletal motor nerve. Medication was administered for 14 days postoperatively–a) verum Cerebrolysin® IP=12–b) shams NaCl 0.9% IP=11, and c) 7 controls (nil). 2nd Op at day 90 (16 surviving rats) for open proof of reinnervation and its type by a) CMAP, b)Vecuronium® application. Fast Blue® labeling were performed. 10 days later, on the 3rd Op N=15, euthanasia and organ fixation were performed. Extensive histology-morphology examinations were performed in Cluj.

Results: Eight rats showed positive CMAPs. Reinnervation and neuromodulation were demonstrated by counting and comparison of the grafted muscle fibers diameter. Four CAMP- positive- rats received Vecuronium®: 1 CERE and 1 NaCl each demonstrated a loss of amplitude respectively two an incomplete muscle blockage due to the coexistence of glutamatergic and cholinergic neurotransmission. Confirmation of the VGluT2 in axons was observed by immunofluorescence. FB+ neurons were observed in many Rexed laminae in grafted spinal cord, but not in the brain.

Conclusion: The coexistence of graft-induced cholinergic and glutamatergic neurotransmission and a great capacity of lower motor neurons and other types of spinal neurons to regenerate were observed. Because of limited animals, pharmacological neuromodulation requires further investigation.

Keywords: Spinal cord injury; Graft induced neuroplasticity; Axonal regeneration; Cortical-rubrospinal tract; Neurotransmitter switch; Immunohistochemistry; Cerebrolysin®

Abbreviations: GB: Giorgio Brunelli; CC: Cornel Cartoi; CERE: Cerebrolysin®; CMAP: Electrical Compound Muscle Action Potentials; DM: Dafin Muresanu; GB: Giorgio Brunelli; HPF: High-Power Fields; IOAM: Internal Obliquus Abdominus Muscle; KvW: Klaus RH von Wild; ML: Marlene Löhnhardt; NMJ: Neuromuscular Junction; NG: Nerve Graft; NR: Neurorehabilitation; PNG: Peripheral Nerve Graft; RCT: Randomized Controlled Trial; SC: Spinal Cord; SCI: Spinal Cord Injury; SNG Sural Nerve Graft; TvW: Tobias von Wild

Introduction

To date, traumatic paraplegia by severance of the spinal cord (SC) remains an irreversible functional clinical condition [1-8]. The issue remains to identify and reverse the conditions that limit regeneration after spinal cord injury (SCI), at which time a hierarchy of "intervention-strategies" is required to restore supra-segmental control through central plasticity and to foster neuroregeneration and neuro-recovery of voluntary function [4-8]. This goal has been successfully achieved both in macaques and in paraplegic human restorative surgery by Brunelli's concept of autologous nerve grafting procedures with direct neurotization of paralyzed muscles in 2000-2002 [9-11]. It is still difficult to understand Brunelli's paradigm (Figure 1), which has demonstrated that the re-establishment of voluntary isolated muscle activation in humans is not replicated elsewhere, despite strenuous effort over the prior decade focused primarily on transdisciplinary treatment [1,2,12].

***Corresponding author:** Klaus RH von Wild, Medical Faculty, Westphalia Wilhelm's University Münster, Münster, Germany, Tel: 491753640400; E-mail: kvw@neurosci.de

Received September 04, 2017; **Accepted** October 11, 2017; **Published** October 16, 2017

Citation: Von Wild KRH, Catoi C, von Wild T, Brunelli G, Muresanu D, et al. (2017) New Aspects of Graft-induced Central Plasticity and Neuroregeneration at T 10 in a Rat Model. J Neurol Neurophysiol 8: 450. doi:10.4172/2155-9562.1000450

Apparently, combinatorial strategies are needed that are based on concepts of nerve grafting and pharmacological neuroprotection to enhance central nervous plasticity and neuroregeneration to overcome the scar-related non-permissiveness of the completely lesioned spinal cord tissue. The aim is to reestablish target-oriented axonal sprouting, neuroregeneration, and neuro-recovery. The combination with biological cell transplants has been shown to be effective in restorative surgery with functional electrical stimulation and intensive physical rehabilitation utilizing modern concepts [11-33]. The prospective clinical study on spinal cord repair, chaired by Young [3] (personal communication Brescia, 04.12.2015), has shown some evidence for the efficiency and effectiveness of intensive physical neurorehabilitation (NR) in Kunming, PRCh, which consisted of 6 to 8 h of walking exercise daily for paraplegic patients [13]. Every endeavor has to be made to facilitate the restoration of voluntary functioning and independent social outcome [1-3,11-33]. However, in our experience, tiring daily physical exercises are also renowned for being one of the most important contraindications in restorative SC surgery. To date, despite some hope for human cures at the basic science level, no experimental evidence has been recommended and translated into clinical applications [1,3,10,11,13,25-29,32]. Based on Brunelli's (GB) many years of experiences in animal research and successful but still limited applications in human paraplegics in 2000-2002 [10], the replication and critical review of GB's grafting procedure in rats was undertaken to obtain scientific proof for the neurophysiological evidence supporting the establishment of this special research model in Luebeck. Our aim was to gain new insight and a better understanding of graft-induced central plasticity to improve neuroregeneration and neuro-recovery in human restorative surgery for traumatic spinal cord and brachial plexus lesions. (11, 14-21, 28-33).

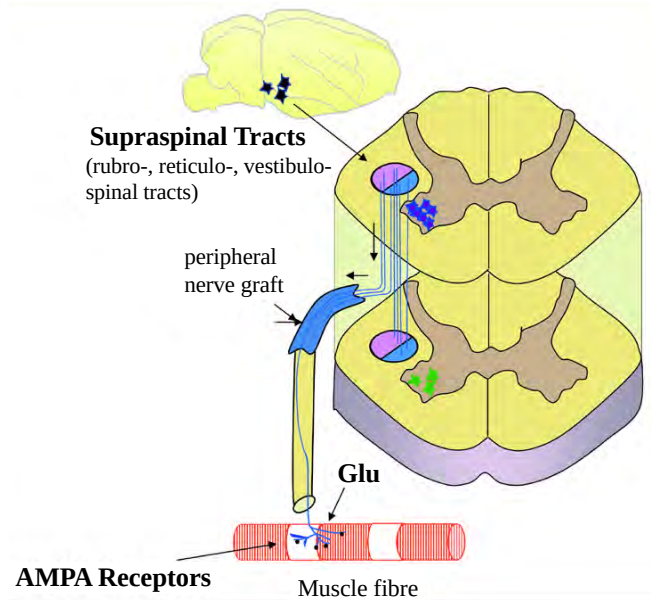

Figure 1: Brunelli's Paradigm "Graft induced Glutamate Neurotransmitter Switch at the neuromuscular junction (NMJ) of skeletal muscle (Brunelli's CNS-PNS grafting paradigm: This sketch shows bridging the 1st cortical motoneuron (glutamatergic) from descending spinal motor pathways from the lateral rubro-reticulo-vestibulo spinal tract) directly to the distal part of the bisected (excluded) 2nd spinal motoneuron (cholinergic)via autologous sural nerve graft for adaptation to the bisected muscular nerve near the NMJ, leading to graft induced Glutamate (GLm) neurotransmitter switch at NMJ (by courtesy Pizzi et al. [72]).

Material and Methods

Study design

Brunelli's spinal cord grafting procedure was replicated in the rat model at the veterinarian surgical laboratories by TvW, supported and under survey of Prof. Dr. Peter Mailänder, Director of the Department of Plastic and Hand Surgery, Burn Intensive Care Unit, UK-SH, Campus Luebeck. TvW had learned the original microsurgical grafting procedure assisted by GB in Brescia, I (Figures 1-3). He was familiar with the perioperative care and postoperative intensive care treatment and housing [33-36]. This challenging research project was designed as an international

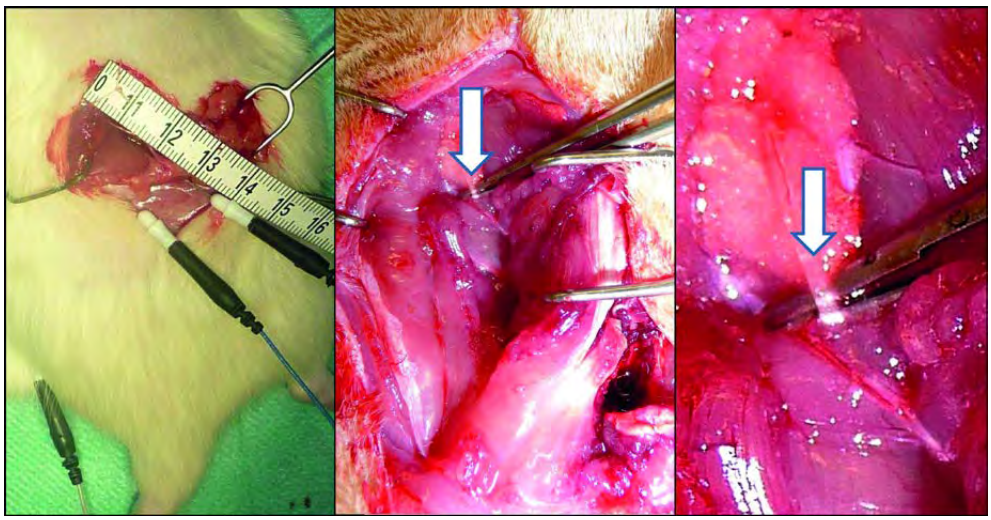

Figure 2: First operation the grafting procedure (prone position): 3rd step microsurgical Identification of the skeletal nerve of right internal obliquus abdominal muscle (IOAM) (Left: A right paravertebral skin incision was made to prepare the right internal obliquus abdominal muscle (IOAM) down to the spine T 12, where the muscle was cut to identify the IOAM nerve. Before the muscle nerve was bisected near the neuromuscular junction (NMJ) the function of the nerve was first tested by open electrostimulation then the distal nerve stump was connected end-to-end with the distal part of SNG and fixed by one stich 9-0 atraumatic. Middle: exposure and electrical identification of the nerve (white arrow) by bipolar electrostimulation, CMAPs (2 mA and 3 mA). Right: Under higher magnification demonstration of the muscle nerve next to its neuromuscular junction just before nerve bisection and graft adaptation at the distal nerve stump (Figure 3).

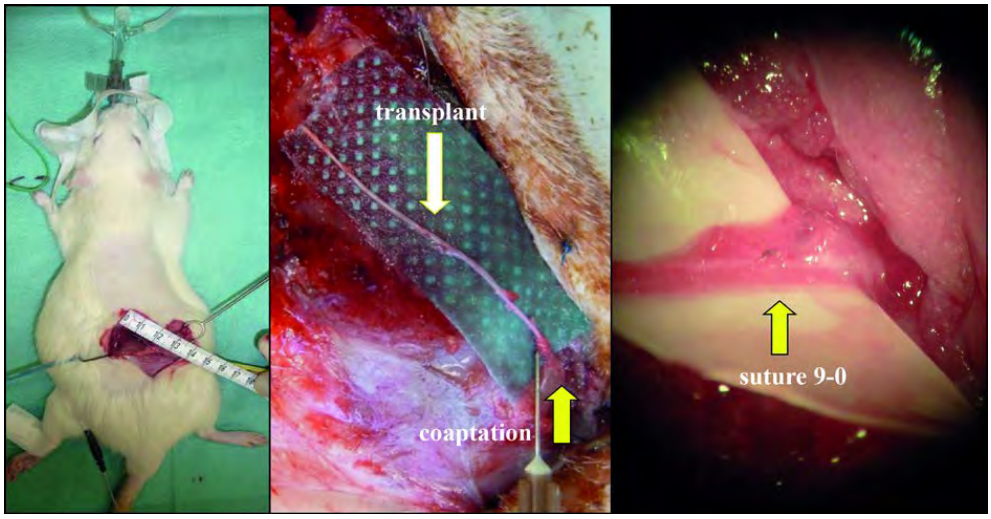

Figure 3: 2nd Op 3 months after grafting procedure (prone position): Revision of the transplant, proof of functional muscle reinnervation and type of neurotransmission/ reinnervation (Microsurgical revision of the transplant under general an aesthesia (No 28, CERE). Rat in prone position, intubated. Left: skin incision for re-exploration level T 12. Middle shows the intact transplant (white arrow), regular co-adaptation (yellow arrow). Right higher magnification: co-adaptation, one stich 9-0 in place (arrow) next to NMJ. exploration of the transplant from the spine to NMJ was performed. Open electromyography was used to evaluate electrical muscle action potentials (CMAP) as a proof of functional reinnervation of the IOAM in situ (Biomed®, Nicolet Biomedical, Madison, WI) 43,44 .Vecuronium® IV was administered in four rats (No 19 NaCl,, 21 CERE, 28 CERE, 29 Na Cl).CMAP revealed the expected muscle reinnervation. So Vecuronium was applied during artificial ventilation that caused loss of CMAP amplitude (Figure 4). This is the proof for graft induced GLu neurotransmitter switch at the NMJ. Direct application of Fast Blue distal the co-adaptation after incision of the nerve stump next to NMJ (Figure 11).

European transdisciplinary, prospective, experimental, double-blinded randomized placebo-controlled study, RCS [37]. The study was conducted in compliance with the National Research Guide for the Care and Use of Laboratory Animals and ethically approved by the Animal Research Committees of the University of Schleswig-Holstein county, D (Research number: V 312-72241.1 [22-25]). Governmental approval and control of legality was obtained from the Animal Protection Officer, Dr. Buttchereit, Institute of Animal Breeding and Husbandry, Christian-Albrechts-University, Kiel, on behalf of the governmental Department of Agriculture and Natural Environments 24062- Kiel, Schleswig-Holstein, D, and in compliance with the European Commission Directive 2010/63/ EU replacing the 1986 Directive 86/609/EEC, which covers the specific legislation for the use of animals for scientific purposes.38 All efforts were made to minimize the suffering of the animals and the number of animals used when only 30 adult white female Sprague Dawley rats were sanctioned (Charles River, 220 to 280 g) [33-38].

Synopsis of the medication: Simple randomization for CERE (verum) and NaCl (shams) for double-blinded application and the identification of controls (nil) was performed by the veterinarian assistant on behalf and under auspices of the veterinarian physician in charge, Dr. Noel. He used the most common and basic method of simple randomization by flipping a coin for our two treatment groups (shames versus treatment) which determined the assignment of each subject [1,18,19,22,34-42] Randomization was for 30 animals [37,38,40-42]. Medication was dependent on the rats physical and behavioral stat on the day of testing (1st Op). It happened that the veterinarian assistant postponed an animal for another day by choosing at random another animal. Both surgeon TvW and his assistant ML did not know about the fluid content during IP injections. The injections for IP administrations looked similar over 14 days. CC and his team were blinded too when they received and archived the animals tissue samples (running numeral 1-30 and/or alphabetic characters) until all histology-morphology examinations has been completed, reviewed, and definitively assessed by CC (Table 1). At the end, when the animals were unfold for medication after some years, they were 12 Cere (verum), 11 NaCl (placebo) well randomized, and 7 controls (nil) (Table 2-4).

General anesthesia [39-42] Preoperatively, all animals were pre-conditioned for at least one week while being housed in the veterinarian laboratories to become familiar with the new environment and staff, such as the stockman and surgical team, regarding their actual and intended special manipulations [34-36,40], e.g. feeding and drinking, being taken out of the box and placed and fixed on the operating table, being placed into a veterinarian CO_2 insufflation box for sedation prior to the general anesthesia procedures for the 1st, 2nd, and 3rd operations [35,36,39-41]. A synopsis of the indications for all pharmaceuticals and biochemical products, their structures, applied dosages and routes of administration, and the different producers are summarized in Table 1 [34-40]. Cerebrolysin® peptidergic drug is composed of porcine brain proteins, with a mixture of 75% free amino acid and 25% low-molecular-weight peptides and is produced by EVER Neuro Pharma GmbH, A-4866 Unterach, A [1,18,19,22,23]. 100 days after the grafting procedure the 3rd operation - euthanasia - was performed only under deep general anesthesia by intraventricular injection of KCl 1-2 mq/kg IV (in phosphate-buffered saline (PBS) solution through the left ventricular heart catheter), followed by 4% paraformaldehyde perfusion via the left ventricular catheter over 30 min before exposure of the organs (SC, sural graft, total brain, and both IOAMs) (Table 1) [33-43].

Surgical equipment: Common microsurgical instruments that are usually used in the veterinarian operating room (OR) were as follows: Leica Wild M-690 Surgical Microscope®; Biomed® atraumatic bipolar electro muscle and nerve- stimulator (Neuro-Pulse®, Bovie Medical Corporation, Florida, USA); Ethilon® monofil 9-0, 10-0 (not absorbable), Vicryl® 3-0 (absorbable; Manipler® wound closure staple gun AZ 35 W 35 B 6,9 mm, H 3,6 (Braun Melsungen, Germany). Artificial ventilation was performed using a mechanical animal ventilator (Biegler Medizin Elektronik), Pmax: 18 mbar, ventilation frequency–50/min, flow–1.5 l/

Indication	Medication Trade names	Pharmaceutical Bio Chemicals	Dosage	Application	Producer
Sedation	CO_2 ≥ 99,5 % insufflation combined with 30% O_2	Carbon dioxide (CO_2) inhalation	CO_2 combined with O_2 30 %	Inhalation box	gas container, Linde Gas 49186 Ostenfelde, D
Ether inhalation sedation, before operation	Ether pro narcosi 50 ml	Diethylether pro narcosi	Drop-inhalation until sedation and sleep	Inhalation Surgical mask	Pharmacy of Univ. Hospital Lübeck, D
Local anesthesia	Scandicain® 5 ml 2 %	Mepivacain 2 mg/ml	1 ml/dosage intraoperative	SC IM	Astra Zeneca London, GB
General anesthesia 1st 2nd, and 3rd Op -euthanasia (at day 1, day 90, day 100)	Ursotamin® 100 ml Rampun® % Ad us. vet. Ketamin/Xylazin rat cocktail ad us. vet. for rats	Ketamine 100 mg/ml Xylazinum 20 mg us. vet. Ketamine 91 mg/kg Xylazine 9.1 mg/kg	100 mg/kg intraoperative 30 mg/kg intraoperative 0.1 ml/100 g and 0.1 ml/100 g rat wt.	IP IP IP	Serumwerk Bamberg AG, D Bayer AG, Leverkusen, D
Neuromodulation - protection, - regeneration - recovery	Cerebrolysin® (CERE)	Peptidergic drug of porcine brain proteins: 75 % free aminoacid, 25 % low molecular peptides	5 mg/kg single dose 25 ml post-operative daily at 14 days	IP	EVER Neuro Pharma GmbH 4866 Unterach AU
Physiological saline solution	Isotonic saline solution NaCl 0.9®	Sodium chloride 0.9 %	5 ml/kg single dose 25 ml postop. daily at 14 days	IP	B. Braun Melsungen AG Melsungen, D
Antibiose	Novaminsulfon® 442,84 mg/ml	Metamizol 500 mg	20 ml drops PO in alert animal postopratively	PO for 10 days	ratiopharm GmbH Ulm, D
Antibiose	Doxycyclin-ratiopharm® SF 100 mg/5 ml	115,4 mg Doxy-oxycyclinhyclat 100mg Magnesium chlorid,	10 mg/kg 2x daily postop.	IV for 6 days	ratiopharm GmbH, Ulm, D
Competitive ACh-neuromuscular blocking	Vecuronium Inresa® 10 mg/5 ml	Vecuronium bromid 10 mg/5 ml=Vecuronium Kation 8.75 mg/5 ml	0.04 – 0.05 mg/kg	IV	Inresa Arzneimittel GmbH Freiburg, D
FB+ for retrograde neuronal tracer motoneu-ronal labeling perikaryons	Fast Blue® (FB) 2,5 %=2,5 mg/ml	Fast blue (FB) fluorescent dye Excitation Wave length: 365 nm Emission 420 nm	2,5 mg/ml	Local appl.	Polysciences Europe GmbH, 69493 Hirschberg, D
Euthanasia for harvesting brain, SC, PNG, IOAMs	KCl-injection 1–2 mg/kg	Kaliumchloridin in phosphate buffertsaline (PBS)	1–2 mg/kg via ventricular catheter	IV intra-ventricular	Pharmacy of Med. Faculty Luebeck, D
Fixation of tissue for histology-morphology	Formaldehyde 4 %	Formaldehyde 4 % solution	30 min perfusion via left ventricle catheter	IV intra-ventricular	Pharmacy of Med. Faculty Luebeck, D

Table 1: Synopsis of indications for pharmaceuticals and biochemical products, their structures, applied dosage, and route of administration for experimental research in rat model [34-42].

Multidimensional Histology	MW Statstic	MW	95,00%CI	N1/N2	P
NNTXDIAM	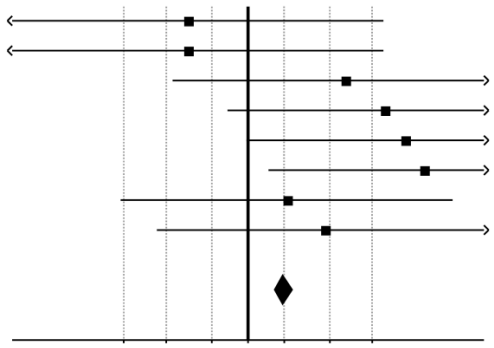	0,4000	(0,0704 to 0,7296)	10 / 3	0,4146
NNTXAREA		0,4000	(0,0704 to 0,7296)	10 / 3	0,4936
NNTXAXON		0,6667	(0,3738 to 0,9596)	10 / 3	0,1928
NNTXMYELIN		0,7333	(0,4660 to 1,0000)	10 / 3	0,1020
NNTXMIN		0,7667	(0,4988 to 1,0000)	10 / 3	0,7533
NNTXMAX		0,8000	(0,5362 to 1,0000)	10 / 3	0,9017
NNTXTOTAL		0,5667	(0,2855 to 0,8479)	10 / 3	0,2347
NNTXCUMUL		0,6333	(0,3476 to 0,9191)	10 / 3	0,3505
Combined (Wei-Lachin)		**0,5611**	**(0,5456 to 0,5766)**	**10 / 3**	**<0.0001**
	0,29 0,36 0,44 0,5 0,56 0,64 0,71				
	Favours “Stimulus No” Favours “Stimulus Yes”				

Table 2: Statistical analyses multidimensional histology – evidence by histometric evaluation (Statistical analyses multidimensional histology to evaluate correlation of muscle fiber diameters with regard to positive motor-reinnervation as it has been intraoperatively demonstrated by positive electrical CMAP. Multidimensional Histology, Wei-Lachin Procedure, Stimulus “Yes” vs. Stimulus “No”, Effect Sizes and two-sided 95%CI*. The combined result of the histological assessments shows significant superiority of the “stimulus yes” group of animals versus the “stimulus no” group (MW=0.5611, 95%CI 0.5456–0.5766, Wei-Lachin procedure, directional test, exploratory interpretation. *Restricted precision of test procedures due to low sample size).

min, inspired oxygen fraction (FiO_2)–0.7) for a duration of 15 to 25 min. A warm circulating water blanket was used intra- and postoperatively to prevent hypothermia by maintain the body temperature of the rats within the physiological range [11,33-36].

Surgical procedures: 1st Op grafting procedure, prone position, three steps: a) The right sural nerve graft (SNG) with a length of approximately 50 mm was harvested. b)After the introduction of a 50 mm longitudinal medial incision and laminectomy T 10–L1, incision of the dura mater and of the arachnoid membrane of segment T 10; a dorsolateral right freehand stitch incision of the SC was created (1.5 to 2 mm deep) at T 10-11, directed toward the dorsolateral funiculus (dlf), and the proximal tip of SNG was introduced towards the lateral corticospinal (lcs), medullary reticulospinal (mrs), and rubrospinal (rs) tracts (for morphology see Figure 7). c) Bisection and end-to end adaptation of the

Muscle Assessments	MW Statstic		MW	95,00%-CI	N1/N2	P
Muscle Marlene	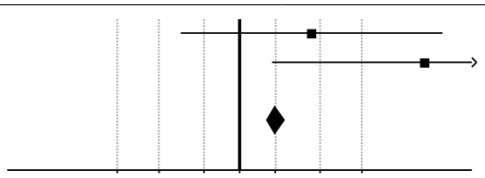		0,6250	(0,3993 to 0,8507)	16 / 5	0,4146
Muscle Catoi			0,8182	(0,5578 to 1,0000)	11 / 2	0,4936
Combined (Wei-Lachin)			**0,5611**	**(0,5456 to 0,5766)**	**10 / 3**	**<0.0001**
	0,29 0,36 0,44 0,5 0,56 0,64 0,71					
	Favours "Stimulus No"	Favours "Stimulus Yes"				

Table 3: Muscle Assessments, Wei-Lachin Procedure (Evidence for favor stimulus "Yes" vs. stimulus "No". Significant effect sizes and two-sided 95%-CI* w respect to the muscle regeneration following grafting using the example of the combined result of the two histological assessments shows significant superiority of the "stimulus yes" group of animals versus the "stimulus no" group (MW=0.5611, 95%CI 0.5456–0.5766, Wei-Lachin procedure, directional test, exploratory interpretation.*Restricted precision of test procedures due to low sample size. *Restricted precision of test procedures due to low sample size).

Case	SNG position*	SC lesions – ipsilateral (I) and contralateral (C)	Areas/grade of axons growth**	Reaction in and around SNG, inside SC	Axons of SNG***, outside of the SC	Fast Blue positive (FB+) neurons****
5 (+)	40^{0}, 1.16 mm *Rxl 7-9*	**I**: WM atrophy (75% *lf*); Wd *lf*	**A**: *Rxl 4-7* (2); *mrs* (2) **T**: *Rxl 7-9* (2)	Gc (2); fibr (2); Sc in SC (1), ang (2); Npres (1).	2,06 (1,04-3,70) 4376	***Th9,10***=8(*Rxl 9)*
6 (+)	35^{0}, 0.52 mm *LSp, IML*	Ec obliteration	**A**: *LSp, rs* (1) **T**: *Rxl 7-9, mrs* (1)	Gc (1); fibr (3); Sc in SC (1), ang (1); Npres (1).	unavailable data few axons	-
10 (+)	15^{0}, 1.29 mm *Rxl 8,9*	**I**: WM atrophy (30% *lf*)	**A**: *Rxl 4-7* (3); *LSp, rs* (2) **T**: *Rxl 8,9* (3)	Gc (3); fibr (1); ang (3); Npres (2); Sc in SC (3).	2,78 (1,53-4,64) 1059	***Th9,10***=1(*Rxl 9)* +1(*Rxl* 5)**;** ***L3***=2(*Rxl 4)*
13 (+)	20^{0}, 0.77 mm *Rxl* 7-9	**I**: WM atrophy (50% *lf;* 20% *vf*)	**A**: *LSp, rs, mrs* (1) **T**: *Rxl 7-9* (1)	Gc (1); fibr (3); ang (3); Npres (2); Sc in SC (1).	unavailable data few axons	***Th11***=9(*Rxl9)* ***L1,3***=3(*Rxl9)* + 2(*Rxl*5) + 4(*Rxl*7) + 1(*D*)
19 (+)	18^{0}, 0.86 mm *Rxl* 7-9	**I**: WM atrophy (30% *lf*)	**A**: *LSp, rs, mrs* (1) **T**: *Rxl 7-9* (2)	Gc (1); fibr (2); ang (2); Npres (3); Sc in SC (1).	1,74 (0,92-3,98) 2959	-
21 (+)	9^{0}, 1.53 mm *Rxl 7-9*	**I**: WM atrophy (80% *lf*, 70% *vf*); Ec dilated	**A**: *LDCom* (2); *dc*(3) **T**: *Rxl 7-10* (2).	Gc (1); fibr (1); ang (3); Sc in SC (1); OB in SNG.	2,44(1,08-7,61) 5161	-
28 (+)	10^{0}, 0.83 mm *Rxl* 5,7	**I**: WM atrophy (10% of *lf*)	**A**: *Rxl 4-6* (3) **T**: *Rxl 7-9* (3)	Gc (1); fibr (1); Npres (2); Sc in SC (1); OB in SNG.	2,42 (1,37-5,45) 3745	-
7 (-)	16^{0}, 1.11 mm *Rxl* 7	**I**: WM atrophy (50% *lf*; 10% *vf*); **I+C:** Wd in *dcs* and *lf*;	**A**: *gr, psdc*, *lf* (3) **T**: *Rxl 7-9* (1)	Gc (2); fibr (1); ang (2); Npres (1); Sc in SC (0)	2,48 (1,13 -5,22) 1411	-
9 (-)	43^{0}, 1.91 mm Contralat. - *lf*	**I**: Wd of *dcs*; **C**: Wd of *dcs*; Ec destruction	**A**: *not found* **T**: *not found*	Gc (3); fibr (1); ang (1); Npres (1); Sc in SC (1)	1,71 (1,09 - 2,36) 1598	-
12 (-)	30^{0}, 0.28 mm Rxl 3,4	**I**: WM atrophy (10% *lf*)	**A**: *Rxl 1-3* (1) **T**: *Rxl 3,4* (1)	Gc (1); fibr (1); ang (1); Npres (2); Sc in SC (1)	3,04 (1,70-6,47) 3275	***L1***=2(*Rxl 9)*
17 (-)	4^{0}, 0.66 mm *Rxl 5*	**I**: WM atrophy (20% *lf*)	**A**: *Rxl 4* (1) **T**: *Rxl 5* (1)	Gc (1); fibr (2); ang (1); Npres (3); Sc in SC (0).	2,32 (1,22-4,08) 1016	-
18 (-)	22^{0}, 0.56 mm *Rxl 5*	**I**: WM atrophy (75% *lf;* 50% *vf*); Wd of *lf* and *vf*	**A**: *Rxl 4* (1) **T**: *Rxl 5* (1)	Gc (1); fibr (3); ang (2); Npres (2); Sc+OB in SC (3)	2,18 (1,29-3,88) 4503	-
23 (-)	0^{0}, 1.11 mm *Rxl 7*	**I**: WM atrophy (50% *dc& lf*); **C**: lymphoplasmac. inflam.	**A**: *gr, psdc* (3) **T**: *Rxl 7-9* (3)	Gc (3); fibr (1); ang (2); Npres (1); Sc in SC (0)	2,05 (1,14-3,84) 8682	-
24 (-)	37^{0}, 0.12 mm *Rxl 2*	No	**A**: *not found* **T**: *not found*	Gc (2); fibr (3); ang (1); Npres (3); Sc in SC (0).	2,11 (1,09-4,42) 5099	-
25 (-)	0^{0}, 0.32 mm *Rxl 2-4*	No	**A**: *Rxl 1,2* (1) **T**: *Rxl 3,4* (1)	Gc (2); fibr. (2); ang (1); Npres (2); Sc in SC (1)	Not found	-
26 (-)	35^{0}, 0.35 mm *LSp*	**I+C:** Wd in *dcs* and *vwc*; **C**: Malacia - Rxl 7	**A**: *Rxl 2,3, rs* (1) **T**: *Rxl 4* (1)	Gc (2); fibr (1); ang.(1); Npres (2); Sc in SC (0)	2,19 (1,02-3,13) 3294	-
27 (-)	0^{0}, 0.32 mm *Rxl 3*	**I+C:** WM atrophy (50% of *dc*)	**A**: not found **T**: not found	Gc (2); fibr (1); ang (1); Npres (2); Sc in SC (0)	2,38 (1,36-2,90) 579	-

Table 4: Histology- Morphology of SC lesion, Areas/Grade of Axon Growth (Histology- Morphology analysis by (by CC) with regard to SC lesion, areas/ grade of axon growth, reaction in/around SNG inside SC, axons of SNG outside des SC, and Fast Blue positive (FB+) neurons. Average diameter of fibers in the oblique abdominal internal muscle).

NG near the IOAM neuromuscular junction that was fixed by using a one stich 9-0 atraumatic (Figure 3). Before being transferred to the ICU, the medication was administered at random as planned [37,42]. 2nd Op was performed at 90 days to obtain intraoperative clinical proof of reinnervation of the transplant and muscular nerve from the spine to the NMJ. Direct (CMAPs) was conducted (Biomed®, Nicolet Biomedical, Madison, WI) (Figures 3&4&5) [43,44]. Oro-pharyngeal intubation for artificial ventilation was performed only when Vecuronium® was to be administered with respect the type of reinnervation/ neurotransmission in rats (No 19 NaCl, 21 CERE, 28 CERE, 29 Na Cl). Finally after the incision of the epineurium of IOAM nerve stump Fast Blue® -soaked-pats were attached around the nerve fascicles, distal to the coadaptation (Figure 3) [11,35-37,40,41].

3rd Op 10 days after Fast Blue® application (N=15): The following organs were harvested upon euthanasia: total brain, SC, the graft, and both IOAMs for extensive histology-morphology examinations.

Electrophysiological diagnostics: (Figures 4 and 5) were performed to identify the skeletal muscle nerve intraoperatively before bisection and subsequently to prove functional reinnervation by CAMP. Vecuronium administered to 4 rats at random showed co-transmission following reinnervation IOAM [42-44].

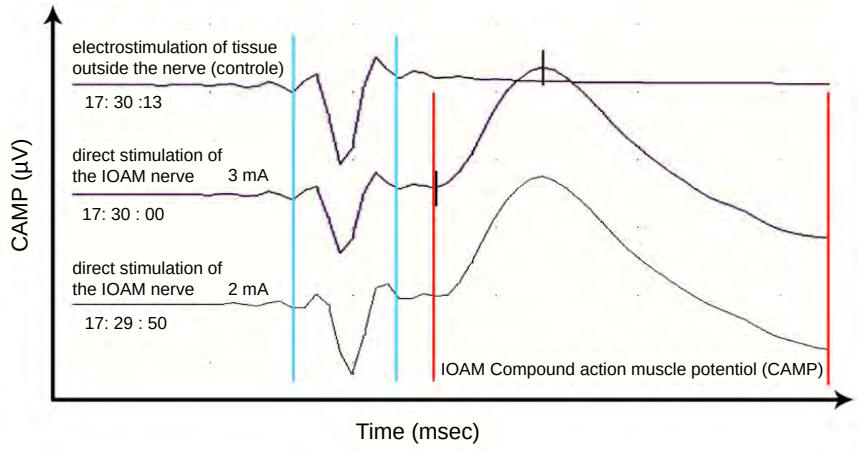

Figure 4: Compound muscle action potential CMAP during bipolar IOAM electro-stimulation (Positive amplitudes demonstrate IOAM re-innervation, as it was the case in 8 of 16 rats t3 months after the grafting procedure. Reinnervation was later on statistically evident by postmortem histometric analysis count of muscle fibers diameter. But, negative CMAP did not exclude positive reinnervation because of technical problems during stimulation, e.g. mismatch).

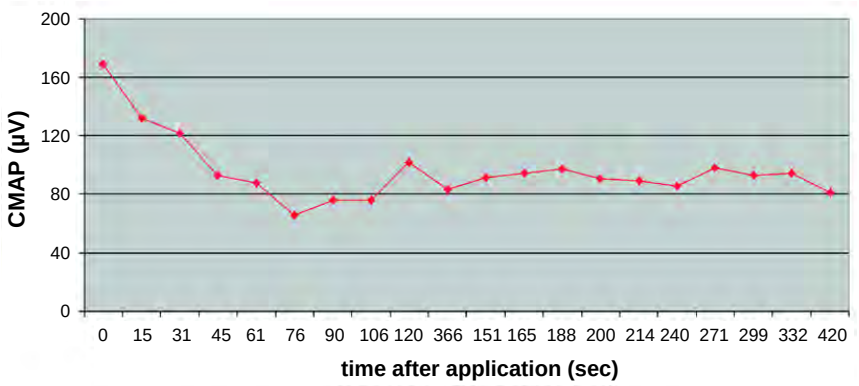

Figure 5: Vecuronium application shows mixed cholinergic/glutamatergic neuromuscular reinnervation (Vecuronium® IV (80 µg/kg) application during artificial ventilation of the rat produce competitive ACh- neuro-muscular blocking for demonstrating the suspected glutamatergic re-innervation of the right IOAM by either decreasing or completely eliminating of the CMAP amplitude, which was measured every 15 sec for 5 min in total. Here in No. 21, CERE, 3 months after grafting, Vecuronium (ACh- blocker) application suspected neuroregeneration of mixed cholinergic and glutamatergic neuromuscular co- transmission type by declining of CMAP amplitude, but no complete loss of electrical potentials (Figure 3).

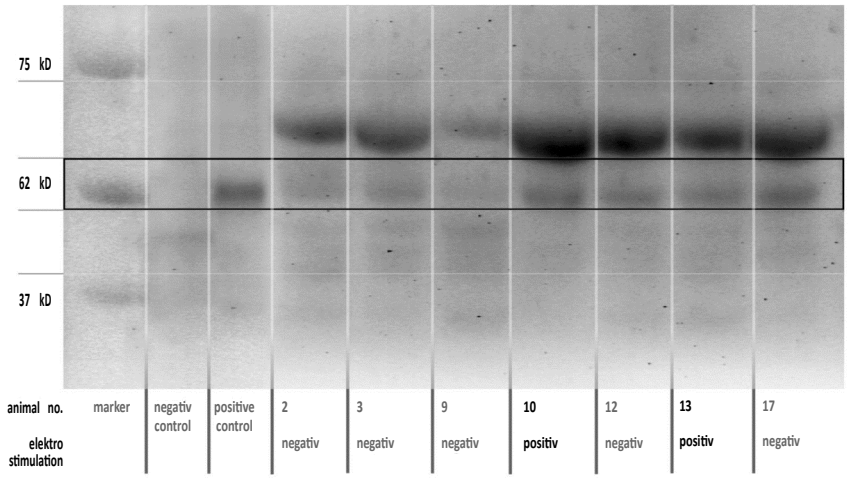

Figure 6: Western Blot: Detection for VGlu 1 transporter in the re-innervated muscle endplates Western Blot: Detection for VGlu 1 transporter in the re-innervated muscle endplates of animals that have been previously “positive” and “negative” both electro stimulated, as noticed later by disclosure of their numbers. This is in contrast to the “functional” definition of re-innervation in so-called negative controls, when no markers appeared.

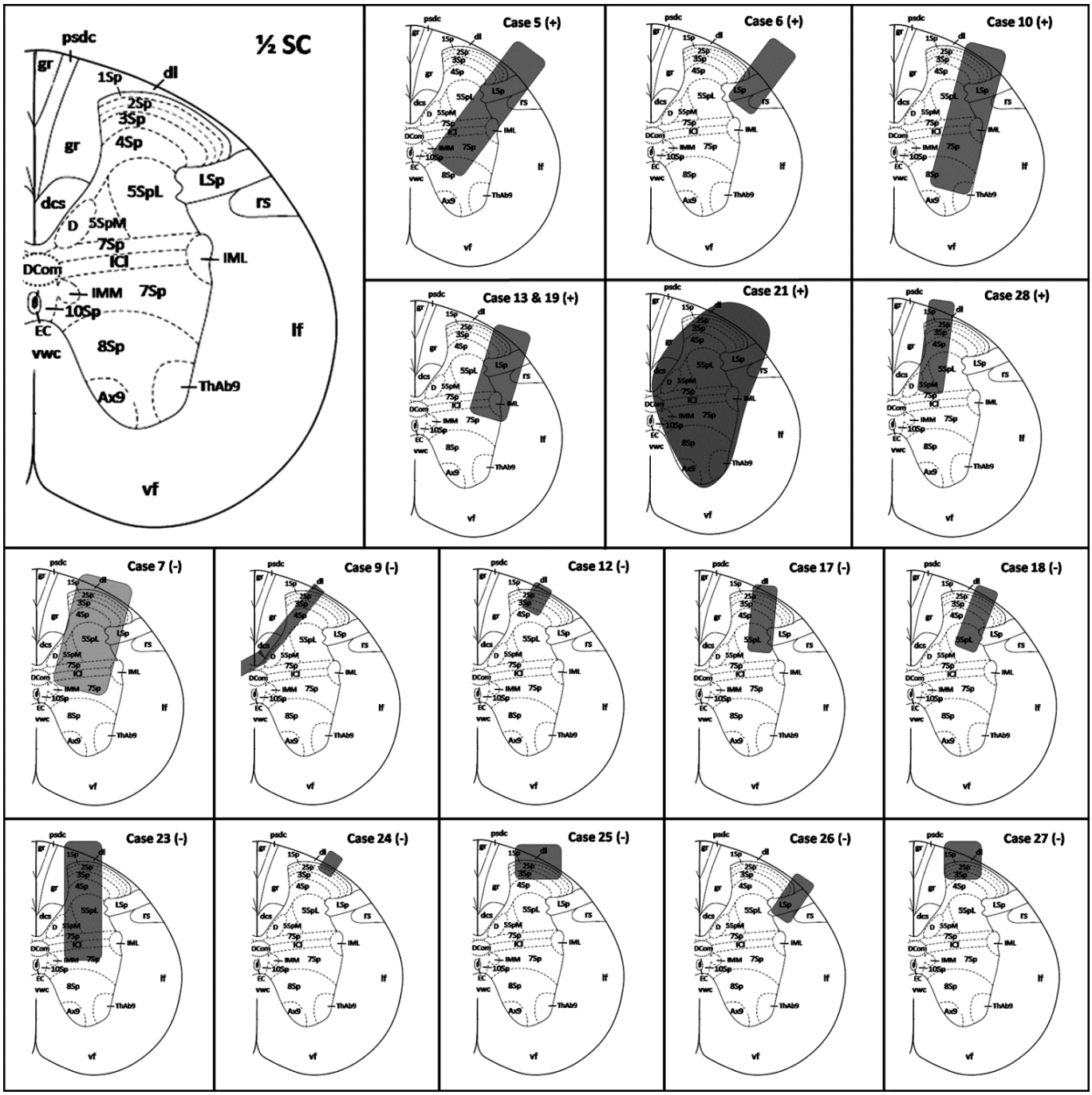

Figure 7: Synopsis graft- positioning by histology- morphology analysis inside the SC at T 10 Positioning of the graft inside the cord was evaluated in each of the 15 surviving cases and additionally in one rat that died at day of revision (No 21 CERE). Only one case, which exhibited a pyogranulomatous inflammation in and around the SC next to the graft segment, was excluded from further review (Table 1) The position of the SNG was considered the entire area in which the former spinal structure was unrecognizable and replaced by the transplanted nerve (regenerated or not) by degenerated/necrotic material and Gc (ceroid-loaded macrophages derived from microglia) and by reactive cell proliferation immediately surrounding the SNG—especially that of Schwann cells, astrocytes, and oligodendroglia. Thus, the grey areas indicating the position of the SNG in each case when spinal tissue was modified and replaced by the NG. Variation in the position of NGs within the SC are as expected for visually guided free-hand insertion. NG positions varied in both depth (ranging from 0.52 mm to 1.53 mm in electromyography (emg) positive cases, respectively, from 0.12 mm to 1.91 mm in emg negative cases that helps to explain the negative results) and angles of insertion from the vertical and median planes (ranging from 9° to 40° in emg positive cases and from 0° to 43° in emg negative cases, more or less same range). A scheme of the final position of the SNG (gray shapes) inside the SC and used abbreviations: 1,2,3…10 - Rexed laminae of spinal gray matter, medial (M) or lateral (L) part, axial (Ax) or abaxial (Ab); D - Dorsal nucleus (Clarke); dc -dorsal columns; dcs - dorsal corticospinal tract; dl - dorsolateral fasciculus (Lissauer); Ec - ependymary canal; gr – gracile fasciculus; ICl - intercalated nucleus; IML - intermediolateral nucleus; IMM - intermediomedial nucleus; lf - lateral funiculus; LDCom - lumbar dorsal common; LSp - lateral spinal nucleus; psdc - postsynaptic dorsal column; rs - rubrospinal tract; vf - ventral funiculus; VH - ventral horn of SC; vwc - ventral white common. (Rexed B 59 Cytoarchitectonic organization of the spinal cord in the cat).

Statistical Methods

It was assumed that no single histopathological measure can capture the multidimensional nature of the neuroplasticity of SC after peripheral nerve grafting [35,42]. In this situation, the use of multiple measures to address the breadth of potential neuroplasticity is recommended, and a multidimensional approach for evaluation of the assessments was chosen for the present study [45]. Minimizing the required assumptions is a recommended approach for confirmatory statements to ensure efficacy, which applies especially in scales with skewed distributions, including floor and ceiling effects. Furthermore, with very small sample sizes, parametric statistics are very sensitive to outliers. Thus, a non-parametric assessment of effects independent of data type and distribution was chosen as the primary analysis method. The analysis was performed by means of the highly efficient Wei-Lachin procedure, a multivariate generalization of the Wilcoxon-Mann-Whitney test. The procedure takes into account the correlation among single variables to produce an overall average estimate and test for differences, as described by Wei and Lachin 1983 and Lachin 1992 [46-47]. Practical examples are provided in modern textbooks on multiple testing problems [48]. Incidentally, it should be noted that the nonparametric Wei-Lachin procedure is similar to the frequently used parametric procedure of O'Brien [49]. We preferred, however, the Wei-Lachin procedure because it is more robust for practical data sets (minimization of required assumptions) [50]. Additionally, the O'Brien procedure has been shown to provide overly liberal results [51]. According to ICH Guideline E9, the results are provided as p values as well as effect-size measures with their two-sided 95% confidence intervals (Mann-Whitney statistic for the corresponding effects size measure of the Wilcoxon-Mann-Whitney test), so that the direction and quantity of the treatment effects were determined with precision [52]. The Mann-Whitney statistic is the most valuable effects-size measure for the Wilcoxon-Mann-Whitney test because it is appropriate when the Hodges-Lehmann shift parameter is no longer valid [53]. The Mann-Whitney effects-size measure (MW) provides the probability that a randomly chosen subject in the test group is better off than a randomly chosen subject in the comparison group, which is defined as follows: P (X<Y) + 0.5 P (X=Y). The traditional benchmarks for the Mann-Whitney effects size measure (MW) are as follows [54]. The level of alpha was defined as alpha=0.05, and a two-sided test was used for superiority. An adjustment for multiplicity was not performed due to the exploratory character of the study. It should be noted that all test results should be interpreted with care due to the very small sample sizes.

Histology-Morphology

Standard procedure for all tissues

Brain, SC, nerves, and IOAM samples were first fixed in 10% neutral-buffered formalin for routine histopathology using paraffin-embedding techniques. The tissue specimens were dehydrated, followed by clarification in xylene and low-melting-temperature paraffin wax embedding. Five-micron sections were cut from each block using a rotary microtome (RM 2125 RT, Leica, Nussloch, Germany), stained with hematoxylin and eosin (HE) and Masson-Trichrome (MT), and then examined under an Olympus BX51 microscope (Olympus, Tokyo, Japan). Images were collected using an Olympus SP 350 digital camera (Olympus, Tokyo, Japan) and processed for counting and measurements using the Olympus Cell B morphometric program. After calibrating according to the real magnification (i.e., pixel conversion to micrometers), semiautomatic counting (e.g., axons, cells, vessels) and measurement of various areas (e.g., nerve diameters, external diameters of the myelin sheaths, and myelomalacia) were performed. This technique was applied to samples collected from the T10-L1 SC segments based on the location of the SNG (approximately 5 mm in each case), the SNGs, the normal nerves, and the internal obliquus abdominis muscles on both sides in all animals.

Scoring system

We had to develop our own scoring system for quantification by counting and measuring the area of the morphologic elements in at least 10 high-power fields (HPF=400x) from serial slides, as demonstrated in (Figure 7). The final score for an element in a given area is expressed as the mean value of the examined fields (Figure 8 A).

Western blot analysis

(Figure 6) was performed on lysates of internal obliquus abdominal muscle (IOAM) with nerve branches from each animal. Proteins from whole tissue samples were extracted. Protein concentrations were determined by the Lowry method (Merck, Darmstadt, Germany). Equal amounts of protein were separated on pre-cast 4-12% Bis-Tris gradient gels (Invitrogen, Karlsruhe, Germany) and transferred onto polyvinylidenedifluoride membranes (Millipore, Eschborn, Germany). Adequate protein transfer was verified by Coomassie blue staining. After blocking the membranes by incubation with skim milk, target proteins were detected by overnight incubation (4 °C) of the membranes with antibodies raised against either vesicular glutamate transporter 1–VGlut1 (Millipore) or vesicular acetylcholine transporter–VAChT (Abcam, Cambridge, UK). After repeated washing, the membranes were incubated with the appropriate horseradish peroxidase-conjugated anti-mouse (GE Healthcare, Freiburg, D) or anti-rabbit IgG (Dako, Hamburg, DL) secondary antibody for 1.5 h at room temperature. Bands were visualized by enhanced chemiluminescence (SuperSignal West Pico substrate, Thermo Fischer Scientific, Bonn, DL with a high-resolution CCD camera (ChemiDoc system and Quantity One software, Bio-Rad, Munich, Germany).

Indirect immunofluorescence assessment of VGlut2

PNG and muscle tissue samples were briefly washed with PBS and cryoprotected by immersion in successive sucrose baths (seven baths, from 10 to 30%, 15 min each). Samples were embedded in OCT (Tissue-Tek, Sakura Compound and Cryomolds), and 10-µm sections were cut on a cryostat (CM 1850; Leica, Nussloch, Germany) at -10°C. Heat-induced antigen retrieval (HIAR) was performed for 3 min in citrate buffer at pH 6.0 using a pressure cooker at 120 °C, and the samples were then cooled for 30 min to room temperature. After a brief wash in PBS, the slides were incubated for [56-60] min in a blocking solution containing 5% goat serum in PBS. The primary antibody - anti-VGlut2 (rabbit polyclonal, Linaris Biologische Produkte, cat. nr. PAK0586), was used at a dilution of 1:100 in blocking solution and incubated overnight (12 h) at 4 °C. The corresponding secondary antibody, goat anti-rabbit IgG conjugated to fluorescein isothiocyanate (FITC; Abcam, cat. nr.ab6717), was then applied to the slides at a 1:100 dilution in PBS for 2 h in the dark. The slides were then briefly washed in PBS and the nuclei were stained with Blue Pseudocolor (DRAQ5) (Cell Signaling, cat. nr. 4084) for 5 min. With the exception of the primary antibody incubation, all incubations were performed in a humidified chamber at room temperature. A secondary antibody control (replacing the primary antibody with 5% goat serum in PBS) and a labeling control (replacing both antibodies and the nuclear stain with blocking solution) were included. Finally, the slides were mounted in an aqueous anti-fade medium (Mowiol-488), sealed with nail polish, and stored in the dark until examined. Indirect immunofluorescence was assessed using a Zeiss LSM 710 Confocal Laser Microscope equipped with Argon/HeNe lasers. Visualization of the immunofluorescence was performed using the 488-nm excitation laser lines with emission filters between 530 and 570 nm for FITC detection. Blue pseudocolor fluorescence was detected using a 543 nm excitation

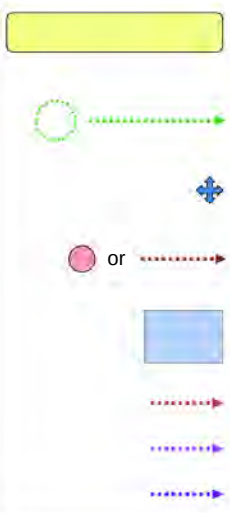

Figure 8A: Graft induced neuroregeneration in histology- morphology (No 10, CERE).
Legend: Symbols and signs used in histology- morphology figures related to rat numbers.
The primary and secondary SC lesions triggered by the surgical procedure (i.e., sectioning, laceration, ischemia, hemorrhage, inflammation, scarring) varied from case to case, depending on the handling of tissue, incision depth, and SNG positioning
We developed a new practical scoring system that allowed us the quantification of histological -morphological and pathological changes by counting and area measurement of the morphologic elements in at least 10 high-power fields (HPF=400x) from serial slides. The final score for an element in a given area is expressed as the mean value of the examined fields. After serially sectioning the entire grafted SC segment, histological examination indicated the position of the SNG in the SC, the lesions induced by the surgical procedures, the reaction of the tissue, and any regeneration. Axonal regeneration/sprouting inside the indicated SC regions was graded as follows: 0 – none (0 axons); 1 – mild (1-20 new axons/HPF); 2 – moderate (21-50 new axons/HPF); and 3 – intense (>50 new axons/HPF). Angiogenesis in and around the SNG inside the SC was graded as follows: 0 – none (0 microvessels); 1 – mild (1 microvessel / HPF); 2 – moderate (2-3 microvessels/HPF); and 3 – intense (>3 microvessels/ HPF). The presence of Gitter cells (Gc) was graded as follows: 0 – none (0 Gc); 1 – mild (1-5 Gc/HPF); 2 – moderate (5-10 Gc/HPF); and 3 – intense (>10 Gc/HPF). The neuronal presence/preservation (Npres) at a maximum distanceof100 µm from the periphery of the SNG was graded as follows: 0 – no neurons/HPF; 1 – mild (1 neuron/HPF); 2 – moderate (2-3 neurons/HPF); and 3 – intense (>3 neurons/HPF). The outgrowth of Schwann cells (Sc) inside the SC from the SNG was graded, taking into account the number of Schwann cells in the bands of Büngner (BB) of at least 3 cells, as follows: 0 – no BB/ HPF; 1 – mild (3-5 Sc /HPF); 2 – moderate (6-9 Sc/HPF); and 3 – intense (>10 Sc/HPF). The quantification of fibrosis in the SNG involved the measurement of areas (in a minimum of five slides and five HPF/slide) and the calculation of the percentage of fibrous tissues without axons in the total area of the SC implant. The epineurium was not considered for measurement. Thus, SNG fibrosis in the SC was graded as follows: 0 – no fibrosis; 1 – mild (<25%); 2 – moderate (26-50%); and 3 – intense (> 50%). The final score of Gitter cells (Gc) infiltration and focal accumulation was variable. Very different histological findings were observed within an individual case from site to site. In the cases with low Gc accumulation scores, areas with massive Gc accumulation and without regenerating/sprouting axons were observed. In addition, cases with high scores possessed areas with few Gc but with many regenerated axons.
Routine histological techniques (e.g., H&E staining) were applied to the entire SC segment adjacent to the graft area and blocked the immune phenotyping of the cells. Although a detailed description of the SC tissue reaction to the graft has not been evaluated and described in more detail by Brunelli and coworkers, we believed that the SC lesions and regenerative reaction to and around the graft had to be adequately quantified and analyzed to take the necessary steps for this kind of research in the future.

line and 661–757 nm emission filters. All images were collected using a Zeiss Plan-Apochromat 63x/1.40 objective. Confocal Images (LSM format) were processed and analyzed using ZEN software.

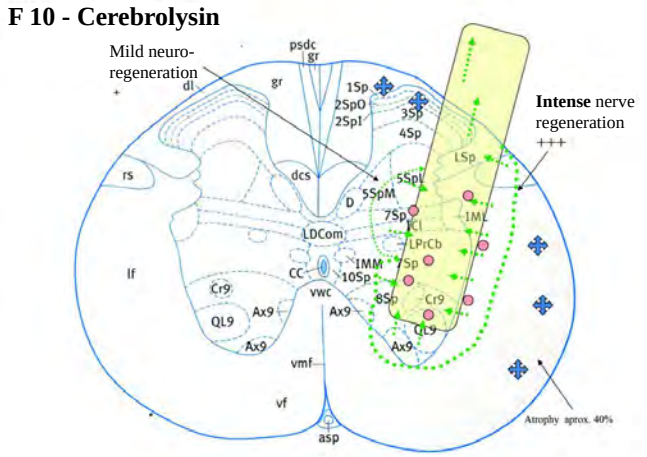

Figure 8B: Histology-morphology T10, No 10 CERE) (Overview of the SNG -marked by black line- in the ventral horn demonstrating an intense growth of axons in the lateral funiculus (lf) - red line; moderate preservation of neurons (N) around the SNG (H&E stain, original magnification 100X). Predominant intense regeneration as well as mild regeneration of PNG, more intense tracts rubrospinal-, pontine reticulospinal-,medial and lateral vestibulospinal- and dorsal corticospinal tracts, rubrospinal and medullary reticulospinal tracts. Atrophy is about 40%).

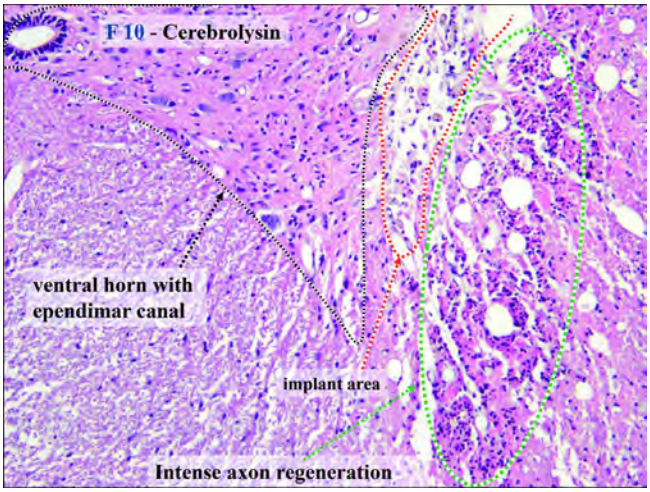

Figure 8C: Overview (H&E stain, 200X) at T 10) Intense axon regeneration-green line Ventral horn with ependymal canal- black line ; red line area of implanted PNG. When analyzing the effect of CERE here in histology and morphology less fibrosis and less scar formation in and around the graft, and less Gitter cell accumulation appeared. Angiogenesis around and in the NG graft was more intense. This is why CERE neuroprotective neuromodulation might be suspected.

Fluorescence microscopy for fast blue tracer

Frozen sections were generated for the entire brain, SC (with the exception of the grafted segments used for routine histology), and nerves. The samples were fixed in 10% neutral-buffered formalin, briefly washed with phosphate-buffered saline (PBS) and cryoprotected by immersion in successive baths of sucrose in PBS (5% sucrose for 30 min, followed by 15% and 30% sucrose for 3 h each, and finally a 1:1 mixture of 30% sucrose and Optimal Cutting Temperature [OCT] embedding medium overnight at 4°C) and then embedded in OCT medium (Poly Freeze, Sigma-Aldrich, D). Frozen sections were obtained using a cryostat (CM

1850, Leica, Nussloch, D) at -20°C and mounted on poly-L-lysine-coated glass slides (Tissue Tack, Polyscience, Inc.). The coverslips were mounted using aqueous anti-fade mounting medium (Mowiol 4–88, Carl Roth, DL). Digital pictures were obtained using an Olympus SP 350 digital camera (Olympus Tokyo, Japan) and processed with the Olympus Cell B program after calibration according to the real magnification (pixel conversion in micrometers). We then performed semiautomatic axon counting and measured the nerve diameter and the external diameter of the myelin sheet (Figure 11). Brain and SC sections were examined immediately after preparation using a fluorescence microscope (Axio Observer A1, Carl Zeiss, DL) at an excitation wavelength of 360 nm for the FB retrograde tracer (410 nm emission wavelength). The microscope was equipped with a video camera (Axiocam HRC), and Axio Vision 4.7 software was used for analysis. Sections containing SNG and former motor nerves were examined using an Olympus BX51 bright field microscope (Olympus, Tokyo, JP). The myelin sheaths appeared as rings that were clearly visible and demarcated in the microscopic field. In our experience, this technique is less time-consuming and provides superior results compared with those obtained using osmic tetroxide.

Results

Surgery

Brunelli's grafting procedure has been replicated: As expected, the overall mortality of 50% was still high but not as high as GB has mentioned concerning his own series in Luebeck 2011. However, GB has not published detailed numbers from his numerous rat experiments, but only mentioned the notable high risk [9-11]. The rats died during our

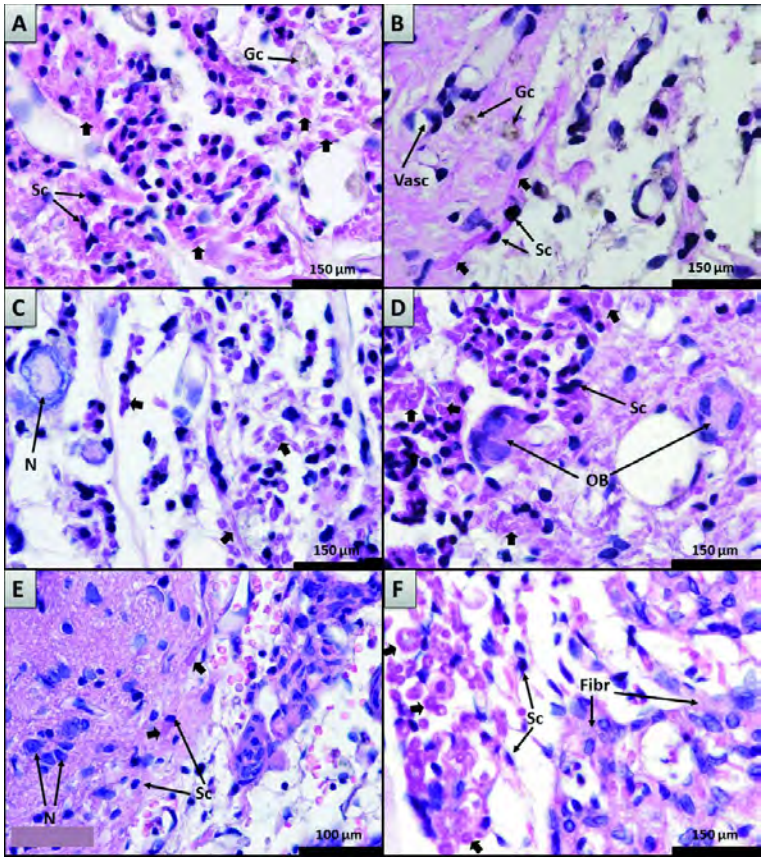

Figure 9(A-F): Detailed histological findings related to SNG regeneration at T 10 (No10 CERE) A. Case 10 CERE – Intense (+++) growth of axons (thick arrows) at the tip of the SNG (area of laminae 7-9); many Schwann cells (Sc) around new axons, peripheral nerve appearance; few Gitter cells (Gc). The outgrowth of Schwann cells from SNGs inside the SC was observed as bands of Büngner that consisted of aligned cell strands that selectively guided regrowing axons.62 These bands contained between several and dozens of cells, and related myelinated axons were observed in all EMG-positive cases. The majority of cases scored 1; an exception was case 10, which scored 3. Six of the ten EMG-negative cases showed no obvious growth of Schwann cells inside SC structures. Three EMG-negative cases scored 1 for proliferation. It is widely known that the Schwann cells play a decisive role in the endogenous repair of peripheral nerves due to their capacity to dedifferentiate, migrate, proliferate, release growth factors, and myelinate regenerated axon.
B. Case 10 – Mild (+) regeneration/sprouting of axons from lamina 9; new axons (thick arrows), intense vascularization (vasc. +++), Sc and Gc;
C. Case 10 – A neuron (N) close to the tip of a transplanted nerve, intense new axonal growth (thick arrows) from laminae 7-9 and moderate vascularization;
D. Case 10 – Intense (+++) growth of axons (thick arrows) from laminae 7-9, many Sc that form an onion bulb (OB) inside the SC matter;
E. Case 10 – Mild (+) growth of axons (thick arrows) from lamina 4, very good (intense, +++) preservation of neurons (N) around SNG, many Schwann cells (Sc) inside of spinal cord matter;
F. Case 5 – SNG outside the SC: very good axonal regeneration (thick arrows) without fibrosis (left part) and intense fibrosis (+++) in most of the SNG (Fibr) (All pictures - H&E stain, original magnification 400X).Angiogenesis around and in the SNG, which is characterized by the outgrowth of capillary sprouts, venules, and arterioles newly formed from pre-existing blood vessels of the SC, was more intense in EMG-positive cases (individual final scores of 2 and 3; score average 2.57) than in EMG-negative cases (individual final scores of 1 and 2; score average 1.3). This observation is not surprising in light of the fact that wound healing is related to angiogenesis, which is regulated by angiogenic signals released in response to hypoxia. Necrosis in and around SC injury lesion sites may be inhibited by effective angiogenesis, and subsequent neuropil protection will enhance recovery, including neural regeneration, after SCI.

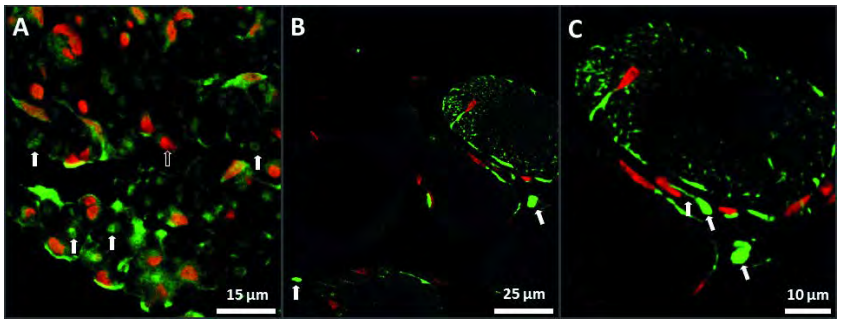

Figure 10(A-C): A (left) No 10 CERE: SNG outside the SC, cross-section: axons with green fluorescence - FITC (white arrows); Schwann cell nuclei red stained - DRAQ5 (empty arrow); B (middle) No 13 NaCl: Abdominal internal oblique muscle, cross-section: axons with green fluorescence - FITC (white arrows); Schwann cell nuclei red stained - DRAQ5; C (right) No 13 NaCl: Detail of picture B: glutamatergic axons and axonal terminals with green fluorescence (white arrows); nuclei stained red; (FITC-conjugated goat anti-Rabbit IgG + rabbit anti-VGLUT2, DRAQ5; Original magnification 630X).

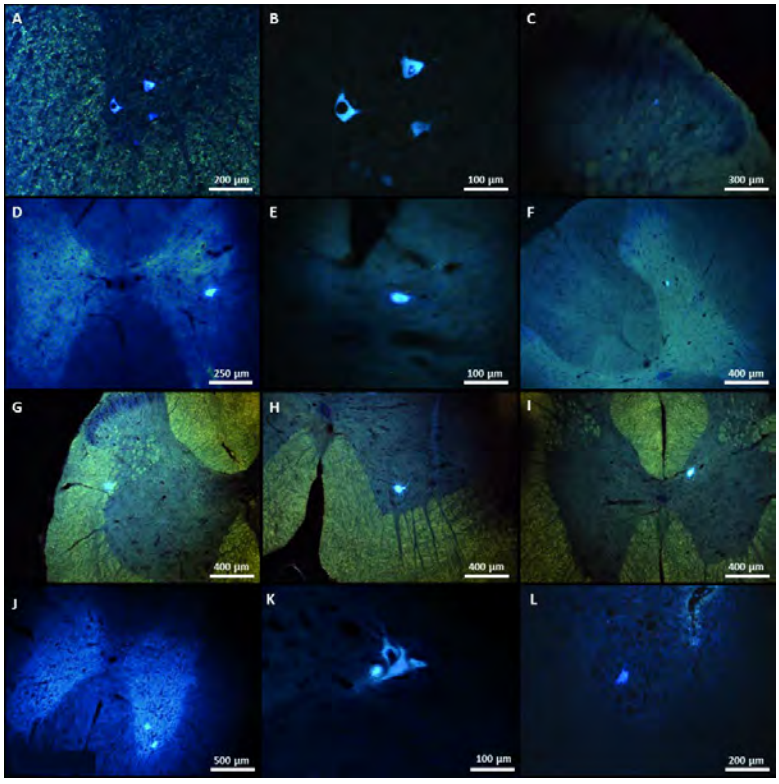

Figure 11 (A-L): FB+ Neurotracer accumulation in different perikaryons of SC (SC examination revealed four cases (three EMG-positive and one EMG-negative case) of neurotracer accumulation (FB+) in the perikaryons (soma) and processes of certain neurons. FB+ neurons were identified in certain segments of the SC that were both anterior (thoracic segments 9-11) and posterior (lumbar segment 1-3) to the site of SNG implantation. The SC segments adjacent to SNG implantation were not examined by fluorescence microscopy because they had been used previously for routine histology. In all FB+ cases, FB+ neurons were observed ipsilateral in Rexed lamina 9. The location (lamina 9) and morphology (multipolar, up to 100µm) of most of these FB+ neurons strongly argue for their classification as alpha motor neurons. In some individual cases (5 and 13), groups of 3 - 4 FB+ neurons were observed on successive slides. Some neurons located in the same lamina were smaller and are presumed to be interneurons (Renshaw cells) or gamma and beta motor neurons.67 In two positive cases (10 and 13), FB+ neurons were identified in other Rexed laminae: laminae 4, 5, and 7 and Clarke's dorsal nucleus (Figure 11). The cells in lamina 4 and Clarke's dorsal nucleus were multipolar and large (60-80 µm). Many cells in lamina 4 respond to light mechanical stimuli, although, nociceptive-specific neurons and neurons with a wide dynamic range are also present.68 Subpopulations of cells in lamina 4 project locally within the SC. The neurons observed in laminae 5 (cases 10 and 13) and 7 (case 13) are theoretically sensitive, respond to noxious and light mechanical stimuli, and could project to other parts of the SC.69

A. & B. No 5 Control: FB+ alpha motor neurons in lamina 9 of the ventral horn of the T 9-10 segment
C. No10 CERE: FB+ neuron in lamina 4 of the L3 segment;
D. No 10 CERE: FB+ neuron in lamina 7 of the Th 9-10 segment;
E. No 13 NaCL: FB+ neuron in lamina 5 of the L1-2 segment; F. No 10 CERE: FB+ neuron in lamina 4/5 of the Th 9-10 segment;
G. No 13 NaCL: FB+ neuron in lamina 5/IML of the L1-2 segment of the contralateral SC;
H. No 13 NaCL: FB+ alpha motor neuron in lamina 9 of L3 segment;
I. No 13 NaCL: FB+ neuron in dnC of the L1-2 segment;
J. No 13 NaCl: FB+ alpha motor neurons lamina 9 of Th 9-10 segment;
K. No 12 NaCl: FB+ alpha motor neuron lamina 9 at L1 segment;
L. No 12 NaCl: FB+ alpha motor neuron in lamina 9 of L1 segment.(UV & bright field).

study at different times without pathophysiological symptoms and signs, e.g., cardiac shock or altered body temperature control. Only one rat, No 4 control, died due to surgical failure (a retroperitoneal perforation at the time of IOAM- nerve preparation). However, this early failure allowed us to improve the atraumatic microsocial approach (Figure 2). Two animals were lost during the 1st Op, and another one died on the same day. One animal each died on days 2, 3, and 5, and two rats were lost on day 10 and one on day 19. Consequently, 21 rats underwent the 2nd Op for transplant revision, when four more animals died immediately after the surgery (No 8, 21, 23, 28), and another two (No 2 and No 3) on the first postoperative day. However, it was possible to save the SC, PNG, and both IOAMs from No 21 and No 28, both of which had received Vecuronium to prove the type of reinnervation by CC (Figure 7, Figure 8, Table 1, Table 2, and Table 3). Fifteen rats completed the total experimental course of 100 days and were sacrificed at the 3rd Op. They were 5 out of 12 CERE (No 10, 11, 17, 24, 27), 7 out of 11 NaCl (No 9,12, 13, 18, 25, 26, 29), and 3 out of 7 controls (No. 5, 6, 7). A few specimens were lost during transport, and some others could not be examined by immunohistochemistry due to previous tissue fixation techniques at the beginning of the study.

Unpredictable sudden deaths

Postmortem assessment by a local veterinarian toxicologist, pharmacologist, and veterinarian pathologist in conjunction with the experienced stockman did not help to satisfactorily explain the sudden insult and death of the 14 rats, both intra- or postoperatively and during long-term professional care. Despite increases in weight and normal drinking and movement observed during housing, these animals were found dead during routine checks, as indicated in the daily protocols. The mode of drug administration (blinded for verum and shames) was later reviewed and discussed with the veterinarian physician Dr. Noel, and the veterinarian pathologist CC, when the medication was revealed and no mismanagement was observed, e.g. an inappropriate medication, incorrect drug dosage, another abdominal perforation, an infection or bleeding. It is likely that cardiovascular and altered body temperature control might have occurred that are known to happen in thoracic spinal cord surgery and in acute SCI [33-36,40,41].

Direct electrical muscle stimulation

After 3 months, during the 2nd Op, electro-stimulation of the PNG transplant in 21 rats was positive in only 8 rats. Out of 4 "electrostimulation positive" animals, two each showed–after Vecuronium® administration–an induced partial / total IOAM block during electrostimulation controls (Figures 3-5, Figure 12); Table 2, Table 3) [43,44].

Postoperative neurological deficits

After the 1st Op and due to surgical grafting manipulation at T 10-12, the animals showed temporary neurological deficits that were more or less pronounced, e.g., ipsilateral lack of leg strength or transient complete flaccid paraplegia. However, these deficits could not be clinically directly related to the cause of death. In general, functional neurological deficits were recovered in all animals to an extent of good neurobehavioral recovery (e.g., regular food intake, climbing, running and stabilization), with increasing body weight starting from day two postoperatively [33].

Caring

At one week preoperatively, the rats were allowed to accommodate to standard conditions of the working environment (including personal touch, mimicking drug administration, and positioning on the operating table and in the box), with free access to chow and water before they were randomly assigned to the three groups for postoperative medication. Treatment issues and special events have been documented in the animal protocol (postoperative caring according to the postoperative neurological deficits). Follow-up housing was provided for three animals in one cage at room temperature of 21 °C, with an air humidity of 50%, 12 h of light-dark, and free water and palette access. Regular assessments of body weight were performed to minimize any suffering from pain or pending neurobehavioral deficits [34].

In comparison to previous studies

Brunelli's Brescia protocol underwent three minor changes: a) the body weights of our rats were lower than 350-400 g; b) abstinence of using an "over the counter" electric heating pad, since these are prone to overheating, as mentioned in the IACUC guidelines [40,41]. Instead we used a warm circulating water blanket intra- and postoperatively to maintain the body temperature within a physiological range (max 37,6 Celsius); c) Fast Blue® was not injected into the muscular nerve to prevent axonal trauma, but it was administered after a small incision of the epineurium by using placing soaked pads directly around at the fascicles at of the distal nerve stump.

Electrophysiological examination CMAP

Open IOAM EMG recordings and electrical neuromuscular stimulation required time and technical skills for the exact positioning of the needle to reduce artifacts by fluid or a non-ideal localization [43,44]. Increasing the current intensity up to 3 mV CMAP was related to regeneration of muscle fibers. Cross-talk artifacts were confirmed by a negative recording at the same distance but only next to the nerve that then demonstrated no signal (Figure 4). In one case, the transplant appeared to be perfectly placed and intact, but stimulation was not possible; the graft might have been incorrectly positioned, which was later proved by histological morphology assessment (Figure 7).

Histology–Morphology

After serially sectioning of the entire grafted SC segment, histological examination indicated the position of the SNG in the SC, the lesions induced by the surgical procedures, the reaction of the tissue, and any type of regeneration. This study was focused on evaluating different aspects of graft-induced central plasticity with regard to neuroregeneration, neuroprotection, cell death, scarring, and positive effects of CERE by pharmacological neuromodulation on functional recovery [18,19,28,29].

Positioning of the SNG

The position of the SNG in the SC was reconstructed through the examination of multiple successive histological slides. Variation in the position of NGs within the SC is as expected for visually guided free-hand insertion. The primary SC injury induced by surgery developed mechanical damage with cell death and bleeding. Additional progressive destruction of the tissue surrounding the necrotic core is known as secondary injury [55-56]. Overview of the right side Rexed laminae comprising a system of ten layers of grey matter (I-X), identified and first described by Bror Rexed [59] to label portions of the grey columns of the spinal cord is shown in Figures 8 and 9. We had to develop a new practical scoring system that allowed the quantification of histological-morphological and pathological changes, by counting and measuring the area of the morphologic elements in at least 10 high-power fields (HPF=400x) from serial slides. The final score for an element in a given area is expressed as the mean value of the examined fields (Figure 8 A). The primary and secondary SC lesions triggered by the surgical procedure varied from case to case. At the time of histological examination, the history of a given lesion was suggested by the myelomalacia (case 26 NaCl), Wallerian degeneration (positive regeneration case 5 control,

negative cases 7, 9, 18, and 26), Gitter cell (Gc) formation (i.e., foci and/or scattered), atrophy of the dorsal columns (NaCl cases 23 and 26), atrophy of lateral and ventral funiculi (most cases), obstruction/dilatation of the central canal (case 6, 9, and 21), neuronal apoptosis (case 23 NaCl), or astrocytosis. In superficially implanted SNG (0.12-0.52 mm), less extensive damage was typically observed (cases 6, 12, 24, and 25, but not cases 26 and 27), in which factors other than surgical section and implant depth were likely involved (e.g., compression, angle of implantation, severed nervous and vascular structures). Routine histological techniques (e.g., H&E staining) were applied to the entire SC segment adjacent to the graft area and precluded immune phenotyping of the cells. Although a detailed description of the SC tissue reaction to the graft has not been evaluated and described in more detail by Brunelli and coworkers, we believe that the SC lesions and regenerative reaction to and around the graft had to be adequately quantified and analyzed to take the necessary steps for this kind of research in future (e.g., less trauma and more precision with the aid of stereotactic graft positioning).

Axon regeneration and sprouting

(AR) around (A) and on the tip (T) of the SNG were demonstrated in all positive cases and in most negative cases (Figure 8). Axon regeneration constitutes the regrowth of transected axons at their cut tip, whereas sprouting involves the growth of collateral branches from fibers that are spared by the injury [55-69].

In our experiments, AR/T could not be differentiated and was observed in multiple areas of the SC. Regenerating and sprouting axons were associated with both NG regeneration and the regeneration of SC structures, such as tracts, laminae, and funiculi. In histological experiments, we considered NG regeneration to be the presence of myelin-covered axons in the SNG. Theoretically, these new axons can regenerate SNGs only by accessing their tip, whereas the remaining SNGs are covered by epineurium that is impenetrable for neuronal buds. Newly formed myelinated axons were observed in various areas of the SC, including Rexed laminae (Rxl) [1-10]. The Rexed laminae comprise a system of ten layers of gray matter (I-X), which is identified by Bror Rexed to label portions of the gray columns of the spinal cord (Figures 8 and 9), the lateral funiculus (lf), the lateral spinal nucleus (LSp), the rubrospinal (rs) tract, the medullary (caudal) reticulospinal (mrs) tract, the dorsal corticospinal (dcs) tract, the gracile fascicle (gr), the lumbar dorsal common (LDCom), and the postsynaptic dorsal column (psdc). However, axon regeneration and sprouting near the tip of the SNG was observed only in Rexed laminae 3-5 (emg-negative cases) and 7-10 (all emg-positive and two negative cases). The intensity (score) of AR/T around and at the tip of the SNG was variable (scored from 1 to 3) [59]. On routine histology, it was impossible to determine the exact origin of axons that grew near or inside the SNG. For example, in case 12 (emg-negative), new axons were observed only in laminae 1-4, but the neurotracer FB was demonstrated in two neurons in lamina 9, indicating at least a partial axon origin. Moreover, spinal neurons possess projections to various laminae of the SC that could be involved in the formation of new axons. Due to the small number of animals evaluated and the wide variety of SNG positions and tissue reactions in the SC, statistical analysis of the positions of the grafts and the area and intensity of axonal growth was not feasible. Although a comparative, statistical analysis of the non-transected nerve was not possible, our results revealed a large number of regenerated myelinated axons of various diameters in SNGs. Although there is evidence that spinal axons grow into the PNG, the number of axons, the thickness of the axons, and their ion channel expression patterns may not be identical to those necessary for typical signal propagation [60]. This finding may explain the limited functional recovery observed during intraoperative electrostimulation.

Angiogenesis

(Figures 8 and Figure 9 B) Around and in the SNG, which is characterized by the outgrowth of capillary sprouts, venules, and arterioles that are newly formed from pre-existing blood vessels of the SC, was more intense in EMG-positive cases.

Gitter cells

Gitter cells were identified around and inside the SNG in all cases (Figure 8 A) [61].

The outgrowth of Schwann cells

(Figure 9) From SNGs inside the SC was observed as bands of Büngner that consisted of aligned cell strands that selectively guided regrowing axons. After traumatic SC injuries, Schwann cells migrate from the periphery into the injury site, where they contribute to endogenous repair processes [63. Other studies have shown that transplanted Schwann cells will not mix with astrocytes; thus, the bridges across injury cavities will not integrate with the SC.5, 64 Our finding that Schwann cells proliferate within the SC seems to contradict these previous studies. Case 18 had a score of 3, demonstrating the formation of an onion bulb (OB) of Schwann cells in the CS structure. Inside the SNG implanted segment, onion bulb formation was identified in three cases: two emg-positive cases (21 and 28) and one emg-negative case [65].

Different grades of SNG fibrosis (from 1 to 3) in the SC were observed in all cases.

However, no statistical correlation was found between the degree of fibrosis and other quantifiable parameters, except with regard to less scarring in the CERE cohort.

Histometric examination

Histometric examination was performed at two different laboratories by ML in Luebeck and by CC in Cluj to evaluate the extent of muscle fiber diameters both in the grafter IOAM and in the contralateral IOAM as proof of graft-induced reinnervation and to determine any statistically significant differences with regard to the effects of CERE medication on neuroprotection and neuro-recovery over three months. The right IOAM showed the expected reduced muscle fiber diameter (atrophy) in all cases, providing proof that the IOAM nerve was bisected before grafting. The degree of atrophy in each case was calculated using the contralateral muscle as a control. Notwithstanding the small number of cases, statistical proof provided clear evidence of muscle recovery by reinnervation analogous to the EMG-positive cases (Figure 12). Even when large variations were observed between the cases, the EMG-positive cases exhibited a larger average muscle fiber diameter compared with the EMG-negative cases, reaching nearly 75% of the contralateral muscle fiber diameter. Although not statistically significant, compared with the two other groups, the CERE rats showed a clear tendency toward larger muscle fiber diameters, as represented and explained herein by the positive values in the chart. However, we must also mention that reinnervation and recovery of the muscle fiber diameters has also been observed in so called "negative" electro-stimulated rats, probably because of technical issues during the intraoperative recording (mismatch). EMG helps to verify the nerve, transplant, and muscle reinnervation, e.g., positive CAMP as an indication of the application of Vecuronium, when the positive amplitude is mandatory for observing any muscular block, but negative electrostimulation does not exclude a positive nerve

transplant with ongoing reinnervation and functional improvement (Table 4 also Figures 8, 9 and 12).

In reality, axonal regeneration is not synonymous with complete functional restoration, and complete or incomplete functional recovery is progressive. Maturation proceeds along the regenerating axon at a slower speed than does axon regrowth and continues for an extended period lasting as long as one year [66]. In addition, muscle atrophy occurs rapidly after denervation, and regaining function and muscle mass after reinnervation is a slow process.

Indirect immunofluorescence

Indirect immunofluorescence assessment of VGluT2 was performed only in EMG-positive cases on PNG and muscle samples, when VGluT2 was observed in many PNG axons. In the right IOAM, positive axon terminals were found only in cases 10 CERE and 13 NaCL. Glutamate is the most important excitatory neurotransmitter in the mammalian CNS. In presynaptic nerve terminals, glutamate is stored in synaptic vesicles and released by exocytosis. Before release of L-glutamate from excitatory synapses, glutamate is transported into synaptic vesicles by vesicular glutamate transporters (VGluTs). Three different VGluTs, (VGluT1, VGluT2, and VGluT3) have been characterized and are considered to represent the most specific marker for neurons that use glutamate as a transmitter. All three VGluTs have been identified in the SC.70 In the SC; VGluT2 mRNA-positive neurons likely belong to interneuron and projection neuron subpopulations. Studies in mouse and rat have shown that motor neurons and neurons in lamina 10 lack VGluT2, at least in the lumbar segment [70]. A previous study argued that the use of PNG in adult rats to join the SC to a nearby-denervated skeletal muscle regenerated the axons of spinal neurons, especially motor neurons and that the neuromuscular junctions were cholinergic because endplate potentials were suppressed by curare [71]. Our experiment morphologically demonstrated the capacity of spinal VGlutT2 neurons to regenerate peripheral nerve grafts and to produce endings (terminals) that innervate skeletal muscle. This finding was correlated with the results of Western blot analyses, which clearly showed the coexistence of two neurotransmitters (acetylcholine and glutamate) in regenerated nerves in the right abdominal internal oblique muscle [72,73].

Fluorescence microscopy

Fluorescence microscopy did not reveal any Fast Blue-positive (FB+) neurons in the brain in either EMG-positive or EMG-negative cases. Instead, SC examination revealed four cases (three EMG-positive and one EMG-negative case) of neurotracer accumulation (FB+) in the perikaryons (soma) and the processes of certain neurons (Figure 11). FB+ neurons were identified in certain segments of the SC that were both anterior (thoracic segments 9-11) and posterior (lumbar segment 1-3) to the site of SNG implantation. The SC segments adjacent to SNG implantation were not examined by fluorescence microscopy because they had been used previously for routine histology.

Statistical Evaluation

With reference to the introduction of statistics in the chapter methods, statistical analyses of histometric data was applied to screen for evidence of muscle reinnervation.

Final statistics were divided and compared for the three arms: CERE, NaCl, Nil. The restricted precision of the test procedures due to the small sample size was taken into account: muscle assessments using multidimensional histology, Wei-Lachin Procedure, stimulus "Yes" vs. stimulus "No", effect sizes and two-sided 95% CI*. The combined results of the histological assessments revealed a significant superiority of the "stimulus yes" group of animals versus the "stimulus no" group (MW=0.5611, 95% CI 0.5456–0.5766, Wei-Lachin procedure, directional test, exploratory interpretation).

Discussion

Traumatic spinal cord injury (SCI) remains among the most devastating injuries that affect the human body [1,11,32]. Until now, traumatic paraplegia by severance of the spinal cord (SC) remains an irreversible condition. Basically, current clinical treatment strategies are targeted to promote axon regeneration and outgrowth beyond the scar formation following SC avulsion [1-5,8-18,20-21,24-31,72-85] Previous experimental and clinical studies together with GB have aroused some hope that paraplegic patients might achieve some selective voluntary muscle reinnervation after grafting the first motor neuron to skeletal hip muscles [10,11,25,72,73].

However, intriguingly this concept of direct neurotization by grafting of target skeletal muscle by supraspinal presynaptic motoneurons to generate functional glutamatergic neurotransmission has not been validated or followed elsewhere. Neuroplasticity can be defined as the ability of the nervous system to respond to intrinsic or extrinsic stimuli by reorganizing its structure, function, and connections. Major advances in our understanding of neuroplasticity have, to date, yielded few established interventions [4-6,42,55-58,77,78,80-86], Brunelli decided on a total neurotransmitter switch at the neuromuscular junction from cholinergic to glutamatergic [11,71-73]. In contrast to the GB group, we did not observe any FB+ neurons in the brain, but we did observe them in many laminae of the SC gray matter. Additionally, we demonstrated the coexistence of graft-induced cholinergic (peripheral) and glutamatergic (central) neurotransmission in reinnervated skeletal IOAM (immunoblotting), which has not been discussed in his previous papers. Taken together, our new observations do not contradict GB's and Pizzi's conclusions, but they do support our hypothesis that PNG regeneration can be mediated by different types of spinal neurons (motor, sensory, interneuron), and therefore coexistence of the two neurotransmitter types is not surprising [87-95].

Further research will be necessary to clarify why GB detected pure retrograde neuronal Fast Blue neurons in the rubrospinal area of the brain, but not in the SC, as observed in our analysis by fluorescence microscopy evidence of Fast Blue-positive (FB+) neurons in the SC in four cases (Figure 11): a) anterior (thoracic segments 9-11) and posterior (lumbar segment 1-3) to those of SNG implantation. In all FB+ cases, the FB+ neurons were observed in ipsilateral lamina 9 - multipolar, up to 100 μm=alpha motor neurons; in two positive cases (No 10 and 13), FB+ neurons were also identified in other laminae (e.g., lamina 4, 5, 7) and in the dorsal nucleus Clarke-sensitive neurons and interneurons. Filli and coworkers suggest [74] that "severed reticulo-spinal fibers, which are part of the phylogenetically oldest motor command system, spontaneously arborize and form contacts onto a plastic propriospinal relay, thereby bypassing the lesion" quote end. These rearrangements were accompanied by substantial locomotor recovery, implying a potential physiological relevance of the detour in restoration of motor function after spinal injury" [75]. The distal segment of a transected nerve is known to undergo Wallerian degeneration and can subsequently regenerate by growth of the proximal axon segment [76]. Thus, in our experiment, the SNG and transected motor nerves completely lost their axons after surgery, a time at which GB and Francolini both postulated that any recovery of nerve function and structure could be attributed to nerve regeneration solely from cortical motor neurons, leading to a total neurotransmitter switch at the NMJ (from cholinergic to glutamatergic transmission) [73]. To our knowledge, GB paradigm has,

to date, never been proved in another research institute. For restoration of direct elective function to occur, new nerve fibers must adopt a trajectory along the growth-promoting tissue [77]. With regard to human applications, we felt committed to ensuring Brunelli's concept using an international transdisciplinary team of experts. The aim of this double-blind, placebo-controlled, randomized study in a rat model was to scientifically retest and review the assumed adaptive central plasticity with exclusive upper motor neurons glutamatergic muscle reinnervation via PNG. Together with our histology-morphology findings, the regenerative capacity of the rubrospinal tract and of lower motor neurons both open new avenues for restorative surgery and voluntary muscle activity after spinal cord lesions. The ability of spinal VGLUT2 neurons to regenerate PNGs and to produce muscular endings (terminals) in the presence of two neurotransmitters (acetylcholine and glutamate) in muscle was demonstrated. These new observations of cord plasticity do not contradict the findings of the two studies reported by GB and Francolini, but they support our hypotheses that PNG regeneration can be provided by different types of spinal neurons (motor, sensitive, interneurons). In general, it has become apparent that combinatorial strategies will be needed to support the central plasticity of axonal sprouting and neuroregeneration. Brunelli's paradigm explained a new concept that has worked for GB and KvW for neuroregeneration and neuro-recovery in human paraplegics. Graft-induced central plasticity and the role of the rubrospinal tract for enhanced sprouting of corticospinal axons demand further research. [93,95].

Many motor and sensory axons grow spontaneously in contused spinal cord, crossing gliotic tissue and white matter surrounding the injury site. Additionally, even sensory axons grow long distances in injured dorsal columns after peripheral nerve lesions [79]. On routine histology, it was impossible for us to determine the exact origins of the axons that grew near or inside the SNG. For example, in case 12 (emg-negative), new axons were observed only in laminae 1-4, but the neurotracer FB was demonstrated in two neurons in lamina 9, indicating at least a partial axon origin. Moreover, spinal neurons possess projections to various laminae of the SC that could be involved in the formation of new axons. Due to the small number of animals evaluated and the wide variety of SNG positions and tissue reactions in the SC, statistical analysis of the positions of the grafts and the area and the intensity of axonal growth was not feasible. Although a comparative, statistical analysis of the non-transected nerve was not possible, our results showed a large number of regenerated myelinated axons of various diameters in SNGs. Nevertheless there is evidence that spinal axons grow into the PNG, the number of axons, the thickness of the axons and their ion channel expression patterns may not be identical to those necessary for typical signal propagation [60], which may explain the limited functional recovery observed during intraoperative electrostimulation.

Young has emphasized the positive effects on neuro-recovery regarding cell transplants by specific medical treatment for neuromodulation, which increases CAMP and neurotrophins, stimulating motor and sensory axons to cross glial scars and to grow long distances in white matter [3]. Spinal cord plasticity can evolve regenerative mechanisms that are normally suppressed by multiple extrinsic and intrinsic factors but can be activated by injury to stimulate neural growth and proliferation [20,21]. The additional beneficial effects of olfactory stem cell transplantation in animal experiments and human SCI, although still limited, have been reported [5-7,26-29,78,85].

We made use of Cerebrolysin® for pharmacological neuromodulation, a drug that has raised hope for the support of clinical neuroprotection, neuro-recovery and neuroregeneration following central nervous lesions [86-92]. Endogenous molecules (e.g., neurotrophic factors) are the most important players involved in CNS protection and recovery. They are able to switch DNA programs. The mechanism of action of endogenous molecules (e.g., Cerebrolysin®) is based on four neurobiological processes: neurotrophicity, neuroprotection, neuroplasticity, neurogenesis, which together target endogenous defense activity (EDA). Cerebrolysin® is a combination of active fragments of different neurotrophic factors that has been shown to increase neuroprotection and neuroregeneration. An advantage is its ability to penetrate the blood-spinal cord barrier. We hypothesized that the acute treatment with CERE resulted in a) cell protection in the region of surgical spinal cord injury by the grafting procedure, b) neuroregeneration, and c) neuro-recovery within both the cord and graft, according to promising reports and evidence from brain and spinal cord lesions [18,19,22,23,28,31,86-94].

When analyzing the present effects of CERE using histology and morphology, we observed less fibrosis and less scar formation in and around the graft, as well as less Gitter cell accumulation. Angiogenesis in and around the NG graft was more intense. The diameters of IOMA fibers appeared to be slightly larger than those observed in non-treated animals. Statistically, the muscle fiber diameters showed a clear tendency toward a positive effect on pharmacological neuromodulation and neuroregeneration (Figure 12). Regarding the small number of animals assessed, this effect was coincidental with the positive electrical stimulation. This observation could be interpreted in accordance with reports showing the influence of CERE on the biochemical mechanism of neuroprotection and neuro-recovery [1,8,18,82-90]. We recommend a new study examining the neuroprotective effect of CERE medication in our grafting procedure model with more extensive CERE treatment up to four weeks and a longer follow up of 6 months, which might provide more detailed insight into its beneficial neuromodulation potency on central plasticity. As suggested by Fouad and coauthors, most studies that have attempted to decode plasticity consider either motor or sensory systems and disregard the contributions of adaptations in both systems simultaneously to recovery and the relevance of changes in each system and their co-dependence [77]. Although there was no way for us to examine sensory recovery in this project, it should be noted that in addition to α-motoneurons, sensory neurons were retrogradely labeled with Fast Blue, which is interesting in light of their potential to aid in sensory and/or motor recovery. Based on our experimental study, we agree with Dopkin's demand that new strategies are needed in neuroscience to improve the transparency of experimental descriptions by uniform reporting standards including centralized databases to facilitate the generation of new hypotheses for testing [80]. In the literature examining detailed technical issues and special benefits, drawbacks concerning in GB's experiences and KvW's personal communication have not yet been reported. However, Brunelli's expertise from his research at the Karolinska Institute and the Department of Primatology, Solana, Stockholm Sweden, led him to choose non-human primates (Macaca fascicularis) for his further research in Brescia, including in his own intensive care unit for postoperative care. We maintained the body temperature of the rats within the lower physiologic range under 37.5°C, and also monitored their fluid balance and body weight. Having been previously confronted in human spinal cord injury treatment with well-known threatening complications regarding unexpected secondary cardiovascular insults during the course of direct surgical procedures within the lower cervical and upper thoracic cord, or during endovascular procedures, cardiovascular shock might be unpreventable. In the rat model, we must also consider the occurrence of the well-known acute hyper/hypothermia dysregulation as cause of death, despite advanced microsurgical skills and strictly obeyed anesthetic guidelines. Although all postoperative animals were dutifully cared for at the intensive care unit, half of them were lost due to suspected cardiovascular shock and thermo-dysregulation. Nevertheless, taking all this evidence into account, even with the limited numbers of animals, it

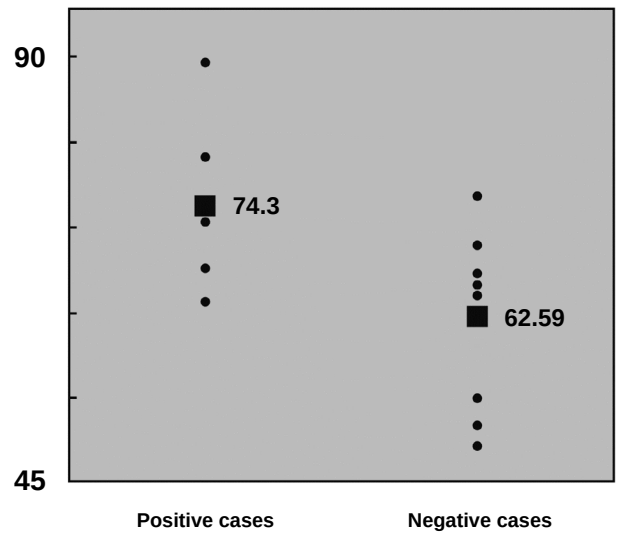

Figure 12: Histology- Morphology of reinnervated muscle fibers for statistical proof reinnervation Average diameter of fibers in the abdominal oblique internal muscle: emg positive and emg negative cases. The values are given as percentages of the control, which was the contralateral muscle for each case without denervation/reinnervation). Statistical evaluation of average diameters of IOAM fibers are shown in comparison with CMAP positive and CAMP negative cases. The values are given as percentages of the control, which was the contralateral left IOAM for each case without denervation. The average per group is represented by the black squares with the related values. Statistically evaluated were all data that have been available from Lüneck, and Cluj, for histiometric count evaluation of IOAM muscle fibers diameters from both sides with regard to reinnervation at the time, when these specimens were still blinded. When specimens were unfolded the statistic shows, although not significant, for CERE treated rats in comparison with the two other groups a clear tendency for bigger muscle fiber diameters as represented here by the positive values.

was possible to provide evidence of successful reinnervation of skeletal muscle by PNG from the thoracic lateral cortical-spinal tract and, above all, to obtain a new understanding of graft-induced central plasticity. This grafting procedure in the rat model has been demonstrated to be a suitable research model for further scientific studies on graft-induced plasticity and pharmacological neuromodulation [42,93-95].

How to prove muscle reinnervation? In addition to axonal regeneration and sprouting in the SC and PNG, neuroplasticity appears to be associated with transmitter modification. Positive EMG potentials were observed in 7 out of the 14 surviving animals. However, missing signals could not be assumed to indicate a negative result in terms of SC plasticity because the detection of fast blue-labeled neurons in the SC or a partial transmitter switch from peripheral cholinergic to central glutamatergic type was shown. Therefore, the combination of histological analysis and electrostimulation served as proof of axon regeneration and sprouting. Moreover, our findings suggest that retrograde fluorescent tracing and immunostaining muscular nervous fibers appear to be more reliable than electrostimulation for confirming experimentally induced neuroplasticity, resulting in muscle reinnervation.

The causes of delayed or failed nerve regeneration seem to include the superficial implantation of SNGs in the SC, overly dorsal surgical access, and vertical positioning touching the dorsal corticospinal tract, gracile fasciculus, or postsynaptic dorsal column, as well as the incorrect direction of the affecting central canal or contralateral gray matter. The best positioning of PNG was achieved via dorsolateral surgical access and dorsomedial positioning at an angle of 30-45° from the vertical line passing laterally to laminae 1, 2, 3, 4 and 5, and the lateral spinal nucleus, such that the tips of the graft extended to lamina 6, 7, or 8. Because the number of animals was too small to be statistically analyzed, we used proven descriptive methods to demonstrate the observed effects [87]. Our results suggest that surgically positioning of the PNGs in the SC in a dorsolateral to ventromedial direction must be sufficiently deep to reach the ventral horn and to induce motor axon regeneration and sprouting. It is known that the growth potential of lesioned axons is more intensive in the case when the injury is closer to the cell body. These patterns support the growth of surviving motoneuron axons into both PNGs and implanted spinal roots. Defined populations of injured SC motoneurons regrow new central axons after avulsion and re-implantation of the detached ventral roots, as demonstrated by both neurophysiological and staining techniques and the restoration of muscle function.

According to our study, spinal motor neuronal processes need to be injured to induce axonal growth that is capable of both regenerating PNGs and motor nerves and restoring muscle function. Upon review of our free-hand PNG implantation, further studies should make use of more precise technical aids and replace the free-hand guidance with an easy stereotactic technology. A second step should be to include a rehabilitation environment for the follow-up.

Conclusion

This transdisciplinary cooperative study shows that replication of Brunelli's free-hand grafting procedure in a rat model is possible. Graft-induced central plasticity will offer even more detailed insight into neuroregeneration, pharmacological neuromodulation and motor nerve recovery with regard to restorative surgery and neurorehabilitation in human paraplegic patients when this experimental research is in the hands of a transdisciplinary team of experts to search for new aspects of SC physiology and the induction of central plasticity with regard to neuro-recovery and neuroprotection. The electromyography, histological–morphology and immunochemical results demonstrated that CNS plasticity permitted muscle reinnervation by spinal neurons from autologous nerve graft procedures when connecting the lateral cortical-rubrospinal tract with a severed skeletal motor nerve. Moreover, spinal motor neurons seemed to be more capable of axonal regeneration and sprouting to regenerate motor nerve and to recover muscle function. The cord plasticity of other spinal neurons was involved in the regeneration of motor nerves, explaining the addition of central glutamatergic axons together with the usual secondary cholinergic phenotype. Schwann cells from PNG were shown to proliferate within the SC, which seemed to be crucial for axonal regeneration. The goal is to directly access the motor neurons of the lateral cortical-rubrospinal tract in SC at a certain thoracic level. As discussed in the literature, pharmacological neuroprotection by CERE treatment requires further experimental confirmation in the rat model. A next step might be another cooperative study that includes postoperative esthesiometry and neurobehavioral assessment over a period of 6 months, including acute pharmacological neuromodulation over six weeks, during which the nerve graft will been positioned even more precisely with the aid of a stereotactic frame.

Acknowledgment

We grieve for Professor Geoffrey Raisman, who passed away on January 27, 2017. He was unable to experience and enjoy the successful conclusion of our many years of scientific research.

This cooperative European experimental research study in rat model is in agreement with the ethics committee Medical Faculty UK-SH Luebeck and in compliance with the European Commission specific legislation 1986 Directive 86/609/EEC that covers the use of animals for scientific purposes. Marlene Löhnhardt contributed to the replication of the GB grafting procedure and, among others, the histometric examination of muscle reinnervation for her doctoral research study.

References

1. Onose G, Mirea A, Padure L, Anghelescu A, Bica F, et al. (2013) Clinical-neurological/ functional assessment in post spinal cord injury patients and current endeavors in achieving of related international standards. Medicine review article. Proc Rom Acad 15: 197-215.
2. Steward O, Popovich PG, Dietrich WD, Kleitman N (2012) Replication and reproducibility in spinal cord injury research. Experimental Neurology 233: 97-605.
3. Young W (2014) Spinal cord regeneration. Cell Transplant 23: 573-611.
4. Bregman BS, Diener PS, McAtee M, Dai HN, James C (1997) Intervention strategies to enhance anatomical plasticity and recovery of function after spinal cord injury. Adv Neurol 72: 257-275.
5. Raisman G, Li Y (2007) Repair of neural pathways by olfactory unsheathing cells. Nat Rev Neurosci 8: 312-319.
6. Carlstedt T (2008) Root repair review: Basic science background and clinical outcome. Restorative Neurol Nerurosci 26: 225-241.
7. Carlstedt T, Cullheim S (2000) Spinal cord motoneuron maintenance, injury and repair. Review. Prog Brain Res 127: 501-514.
8. Cramer SC, Sur M, Dobkin BH, O'Brien Ch, Sanger TC, et al. (2011) Harnessing neuroplasticity for clinical application. Brain 134: 1591-1609.
9. Brunelli G, Milanesi S, Bartolaminelli P, De Filippo G, Brunelli F, et al. (1983) Experimental grafts in spinal cord lesions (preliminary report). Ital J Orthop Traumato 9: 53-56.
10. Brunelli GA (2001) Direct neurotization of muscles by presynaptic motoneurons. J of Reconstructive microsurgery 17: 631-636.
11. Brunelli G, Spano PF, Barlati S, Guarneri B, Barbon A, et al. (2005) Glutamatergic reinnervation through peripheral nerve graft dictates assembly of glutamatergic synapses at rat skeletal muscle. PNAS 102: 8752 - 8757.
12. Ramer LM, Ramer MS, Bradbury EJ (2014) Restoring function after spinal cord injury: Towards clinical translation of experimental strategies. Lancet Neurol 12: 1241-1256.
13. Zhu H, Poon W, Liu Y, Leung GK, Wong Y, et.al. (2016) Phase I-II clinical trial assessing safety and efficacy of umbilical cord blood mononuclear cell transplant therapy of chronic complete spinal cord injury. Cell Transplant 25: 1925-1943.
14. Fawcett JW, Schwab ME, Montani L, Brazda N, Müller HW (2012) Defeating inhibition of regeneration by scar and myelin components. In Verhaagen J, McDonald, JW (eds), handbook of clinical neurology 109: 503-522.
15. Freund P, Wannier T, Schmidlin E, Bloch J, Mir A, et al. (2007) Anti-nogo-A antibody treatment enhances sprouting of corticospinal axons rostral to a unilateral cervical spinal cord lesion in adult macaque monkey. J Comp Neurol 502: 644-659.
16. Fouad K, Dietz V, Schwab ME (2001) Improving axonal growth and functional recovery after experimental spinal cord injury by neutralizing myelin associated inhibitors. Brain Res Rev 36: 204-212.
17. Fouad K, Tse A (2008) Adaptive changes in the injured spinal cord and their role in promoting functional recovery. Neurol Res 30: 17-27.
18. Muresanu DF (2007) Neuroprotection and neuroplasticity-a holistic approach and future perspectives. J Neurolog Sciences 257: 38-43.
19. Muresanu DF, Sharma A, José V, Lafuente JV, Patnaik Ret al. (2015) Nanowired delivery of growth hormone attenuates. Pathophysiology of spinal cord injury and enhances insulin-like growth factor-1 concentration in the plasma and the spinal cord. Mol Neurobiol 52: 837-845.
20. Schwab ME, Barholdi D (1996) Degeneration and regenerartion of axons in the lesioned spinal cord (Review). Physiological reviews 76: 319-370.
21. Schwab ME, Strittmatter SM (2014) Nogo limits neural plasticity and recovery from injury. Curr Opin Neurobiol 27: 53-60.
22. Sharma HS, Muresanu D, Sharma A, Patnaik R, Lafuente JV (2009) Nanoparticles influence pathophysiology of spinal cord injury and repair. Elsevier, Great Britain pp: 154-180.
23. Sharma HS (2010) Selected combination of neurotrophins potentiates neuroprotection and functional recovery following spinal cord injury in the rat pp: 358-364.
24. Stoltz JF, de Isla N, Li YP, Bensoussan D, Zhang L, et al. (2015) Stem cells and regenerative medicine: Myth or reality of the 21th century. Stem Cells Int 34731: 734-731.
25. von Wild K, Rabischong P, Brunelli G, Benichou M, Krishnan K (2008) Computer added locomotion by implanted electrical stimulation in paraplegic patients (SUAW). Acta Neurochir 79: 99-104.
26. Gabr H A, Ghannam O, Awad MR, von Wild K, El-Kheir WA, et al. (2011) Autologous mesenchymal stem cell therapy for spinal cord injury: Long term safety and clinical efficacy. AJNN 3: 100-106.
27. El-Kheir WA, Gabr H, Awad MR, von Wild K, Ramadan M (2010) Autologous mesenchymal stem cells for neuroregeneration after traumatic spinal cord injury: A comparison between bone marrow and peripheral blood populations. Am J Neuroprotec Nuroregen 2: 78-85.
28. Huang H, Sun TS, Chen L, Dimitrijevic, Moviglia GA, et al. (2014) Global clinical neurorestoration in complete chronic spinal cord injury. Neuroreport 25: 144-144.
29. Huang H, Sun TS, Chen L, Moviglia GA, Chernykh E, et al. (2014) Consensus of clinical neurorestorative progresses in patients with complete chronic spinal cord injury. Cell Transplant 23: 5-17.
30. Papastefanski F, Matsas R (2015) From demyelination to remyelination: The road toward therapies for spinal cord injry. Glia 63: 1101-1125.
31. Yilmaz T, Kaptanoglu E (2015) Current and future medical therapeutic strategies for functional repair of spinal cord injury. World J Orthop 6: 42-55.
32. von Wild KR (2007) Restoration of locomotion in posttraumatic paraplegics. The neurosurgeons personal view pp: 59-66.
33. Lemmon VP, Ferguson AR, Popovich PG, Xu XM, Snow DM et al. (2014) Minimum information about a spinal cord injury experiment: A proposed reporting standard for spinal cord injury experiments. J Neurotrauma 31: 1354-1361.
34. NIH guide for the care and use of laboratory animals (2010) NIH publication national academy of sciences. The national academy press, Washington D.C., USA.
35. Slatter DH (2003) Veterinarian surgery. Textbook of small animal surgery 3rd ed. Elsevier Science, USA, Vol. 1, Sounders Philadelphia.
36. Waynforth HB, Flecknel PA (1992) Experimental and surgical technique in the rat. 2nd ed. Academic Press San Diego-UK Elsevier academic press Amsterdam, Boston, Heidelberg, London pp: 100-152.
37. Kabisch M, Ruckes C, Seibert-Grafe M, Blettner M (2011) Randomized controlled trials: Part 17 of series on evaluation of scientific publications. Dtsch Arztebl Int 108: 663-668.
38. (2016) European commission legislation for the protection of animals used for scientific purposes.
39. Francischi JN, Frade TI, Almeida MP, Querioz BF, Bakhle YS (2017) Ketamin-xylazine anaesthesia and orofacial administration of substance P: A lethal combination in rats. Neuropeptides S0143-4179: 30113-30115.
40. IACUC Guidelines: Anesthesia (2016) Office of animal resources institutional animal care and use university of Iowa.
41. Johns Hopkins University (JHU) (2006) Animal care and use policies and guidelines. Use of Ether for animal anesthesia at Johns Hopkins University (Revised by the JHU Joint Health Safety and Environment/Animal Care and Use Committee).
42. Suresh KP (2011) An overview of randomization techniques: An unbiased assessment of outcome in clinical research. J Hum Reprod Sci. 4: 8-11.
43. Smith DC (1992) An evoked compound electromyogram simulator with external microprocessor control facility. J Med Eng Technol 16: 129-132.
44. Kuntzer T, Flocard F, Vial C, Kohler A, Magistris M, et al. (2000) Exercise test in muscle channel neuropathies and other muscle disorders. Muscle Nerve 23: 1089-1094.
45. Rahlfs VW, Vester J (2012) The multidimensional approach instead of testing individual endpoints. Pharm Med 14: 160-165.
46. Wie LJ, Lachin JM (1984) Two-sample asymptotically distribution-free tests for incomplete multi-variate observations. J Am Stat Assoc 79: 653-661.
47. Lachin JM (1992) Some large-sample distribution-free estimators and tests for multivariate partially incomplete data from two populations. Stat Med 11: 1151-1170.
48. Dimitrenko A, Tanhane AC, Bretz F (2009) Multiple testing problems in pharmaceutical statistics. Chapman & Hall/CRC Press, Taylor & Francis Group.
49. O'Brien PC (1984) Procedures for comparing samples with multiple endpoints. Biometrics 40: 1079-1087.

50. LaVange LM, Durham TA, Koch GG (2005) Randomization-based nonparametric methods for the analysis of multicenter trials. Stat Methods Med Res 14: 281-301.

51. Frick H (1997) A note on the bias on O'Brien's OLS test. Biometrical J 39: 125-128.

52. ICH-Biostatistics Guideline (1998) ICH opic E9, ICH harmonized tripartite guidance, note for guidance on statistical principles for clinical trials. CPMP/ICH/363/96.

53. D'Agostino RBSr, Campbell M, Greenhouse J (2006) Non-inferiority trials: Continued advancements in concepts and methodology. Stat Med 25: 1097-1099.

54. Colditz GA, Miller JN, Mosteller F (1988) Measuring gain in the evaluation of medical technology. The probability of a better outcome. Int J Technol Assess Health Care 4: 637-642.

55. Schwab ME, Bartholdi D (1996) Degeneration and regeneration of axons in the lesioned spinal cord. Physiol Rev 76: 19-70.

56. Beattie MS, Li Q, Bresnahan JC (2000) Cell death and plasticity after experimental spinal cord injury. Prog Brain Res 128: 9-21.

57. Darian-Smith C (2009) Synaptic plasticity, neurogenesis and functional recovery after spinal cord injury. Neuroscientist 15: 149-165.

58. Weidner N, Ner A, Salimi N, Tuszynski MH (2001) Spontaneous corticospinal axonal plasticity and functional recovery after adult central nervous system injury. PNAS 98: 3513-3518.

59. Rexed B (1952) The cytoarchitectonic organization of the spinal cord in the cat. J Comp Neurol 96: 414-495.

60. Sandrow-Feinberg HRT, Miller K, Santi L, Connors T, et al. (2009) Peripheral nerve grafts and chondroitinase promotes functional axonal regeneration in the chronically injured spinal cord. J Neurosci 29: 14881-14890.

61. Kundi S, Bicknell, R, Ahmed, Z (2013) The role of angiogenic and wound-healing factors after spinal cord injury in mammals. Neurosci Res 76: 1-9.

62. Ribeiro-Resende VT, Koenig B, Nichterwitz S, Oberhoffner S, Schlosshauer B (2009) Strategies for inducing the formation of bands of Büngner in peripheral nerve regeneration. Biomaterials 30: 5251-5259.

63. Oudega M, Xu X (2006) Schwann cell transplantation for repair of the adult spinal cord. J Neurotrauma 23: 453-467.

64. Afshari FT, Kwok JC, Fawcett JW (2010) Astrocyte-produced ephrins inhibit Schwann cell migration via VAV2 signaling. J Neurosci 30: 4246-4255.

65. Xu XM, Guénard V, Kleitman N, Aebischer P, Bunge, MB (1995) A combination of BDNF and NT-3 promotes supraspinal axonal regeneration into Schwann cell grafts in adult rat thoracic spinal cord. Exp Neurol 134: 261-272.

66. Burnett MG, Zager EL (2004) Pathophysiology of peripheral nerve injury: A brief review.

67. Watson C, Paxino G, Kayalioglu G, Heise C (2008) Atlas of the rat spinal cord. Academic Press pp: 238-306.

68. Cervero F, Handwerker HO, Laird JM (1988) Prolonged noxious mechanical stimulation of the rat's tail: responses and encoding properties of dorsal horn neurons. J Physiol Lond 404: 419-436.

69. Mannen H (1975) Reconstruction of axonal trajectory of individual neurons in the spinal cord using Golgi-stained serial sections. J Comp Neurol 159: 357-374.

70. Brumovsky PR (2013) VGLUTs in peripheral neurons and the spinal cord: Time for a review. ISRN Neurol 1: 829753.

71. Horvat JC, Pecot-Dechavassine M, Mira JC, Davarpanah Y (1989) Formation of functional endplates by spinal axons regenerating through a peripheral nerve graft. A study in the adult rat. Brain Res Bull 22: 103-114.

72. Pizzi M, Brunelli G, Barlati S, Spano P (2006) Glutamatergic innervation of rat skeletal muscle by supraspinal neurons: A new paradigm in spinal cord injury repair. Curr Opin Neurobiol 16: 323-328.

73. Francolini M, Brunelli G, Cambianica I, Barlati S, Barbon A, et al. (2009) Glutamatergic reinnervation and assembly of glutamatergic synapses in adult rat skeletal muscle occurs at cholinergic endplates. J Neuropathol Exp Neurol 68: 1103-1115.

74. Filli L, Engmann AK, Zörner B, Weinmann O, Moraitis T, et al. (2014) Bridging the gap: A reticulo-propriospinal detour bypassing an incomplete spinal cord injury. J Neurosci 34: 13399-13410.

75. Kadoya K, Nguyen K, Lee-Kubli C, Kumamaru H, Yao L, et al. (2016) Spinal cord resconstituation with homologous neural grafts enables robust corticospinal regeneration. Nat Med 22: 479-487.

76. Waller A (1850) Experiments on the section of the glossopharyngeal and hypoglossal nerves of the frog, and observations of the alterations produced thereby in the structure of their primitive fibres. Philos Trans R Soc (Lond.) 140: 423-429.

77. Fouad K, Krajacic A, Tetzlaff W (2011) Spinal cord injury and plasticity: Opportunities and challenges. Brain Res Bull 84: 337-342.

78. Gladwin K, Choi D (2015) Olfactory ensheathing cells: Part I—current concepts and experimental laboratory models. World Neurosurg 83: 114-119.

79. Fulli L, Schwab ME (2012) The rocky road to translation in spinal cord repair. Ann Neurol 72: 491-501.

80. Dobkin BH (2010) What matters in cellular transplantation for spinal cord injury: The cells, the rehabilitation, or the best mix? Neurorehabil Neural Repair 24: 7-9.

81. Haninec P, Houstava L, Stejskal L, Dubový P (2003) Rescue of rat spinal motoneurons from avulsion-induced cell death by intrathecal administration of IGF-I and cerebrolysin. Ann Anat 185: 233-238.

82. Goldberg JL (2003) How does an axon grow? Genes Dev 17: 941-958.

83. Carlstedt T (2016) New treatments for spinal nerve root avulsion injury. Front Neurol 7: 135.

84. Lima C, Escada P, Pratas-Vital J, Branco C, Arcangeli CA, et al. (2010) Olfactory mucosal autografts and rehabilitation for chronic traumatic spinal cord injury. Neurorehabil Neural Repair 24: 10-22.

85. Ibrahim A, Li D, Collins A, Tabakow P, Raisman G, et al. (2014) Comparison of olfactory bulbar and mucosal cultures in a rat rhizotomy model. Cell Transplant 23: 1465-1470.

86. Sharma HS, Muresanu DF, Sharma A (2013) Novel therapeutic strategies using nanodrug delivery, stem cells and combination therapy for CNS trauma and neurodegenerative disorders. Expert Rev Neurother 13: 1085-1088.

87. Muresanu DF, Buzoianu A, Florian SI, von Wild T (2012) Towards a roadmap in brain protection and recovery. J Cell Mol Med 16: 2861-2871.

88. Muresanu DF, Heiss WD, Hoemberg V, Bajenaru O, Popescu CD, et al. (2016) Cerebrolysin and recovery after stroke (CARS): A randomized, placebo-controlled, double-blind, multicenter trial. Stroke 47: 151-159.

89. Poon W, Vos P, Muresanu D, Vester J, von Wild K, et al. (2015) Cerebrolysin Asian Pacific trial in acute brain injury and neuro recovery: Design and methods. J Neurotrauma 32: 571-580.

90. Sharma A, Muresanu DF, Mössler H, Sharma HS (2012) Superior neuroprotective effects of cerebrolysin in nanoparticle-induced exacerbation of hyperthermia-induced brain pathology. CNS Neurol Disord Drug Targets 11: 7-25.

91. Wells JW, Hurlbert RJ, Fehlings MG, Yong VW (2003) Neuroprotection by minocycline facilitates significant recovery from spinal cord injury in mice. Brain 126: 1628-1637.

92. Thomas AJ, Nockels RP, Pan HQ, Shaffrey CI, Chopp M (1999) Progesterone is neuroprotective after acute experimental spinal cord trauma in rats. Spine 24: 2134-2138.

93. Dietz V, Schwab ME (2017) From the rodent spinal cord injury model to human application: promises and challenges. Journal of Neurotrauma 34: 1826-1830.

94. Theisen CC, Sachdeva R, Austin S, Kulic, D, Kranz V, et al. (2017) Exercise and peripheral nerve grafts as a strategy to promote regeneration after acute or chronic spinal cord injury. Journal of Neurotrauma 34: 1909-1914.

95. Brunelli AG, Monini L, von Wild KR (2013) Brain plasticity by multiple single neurons scattered in the brain cortex. Am J Neuroprotec Neuroregen 5: 1-6.